Aus der Klinik für Radiologie
der Medizinischen Fakultät Charité – Universitätsmedizin Berlin

DISSERTATION

Body Composition Analysis: Skeletal Muscle Measurement with Computed Tomography and Implications for Patient Care

Analyse der Körperzusammensetzung: Messung der Skelett-muskulatur mit Computertomographie und Implikationen für die Patientenversorgung

zur Erlangung des akademischen Grades
Medical Doctor - Doctor of Philosophy (MD/PhD)

vorgelegt der Medizinischen Fakultät
Charité – Universitätsmedizin Berlin

von

Georg Fuchs

aus Dresden

Datum der Promotion: 30.11.2023

Preface

I would like to express my sincere gratitude to my doctoral supervisors Prof. Dr. med. Florian J. Fintelmann, Prof. Dr. med. Bernhard Gebauer, and Prof. Dr. med. Patrick Asbach for their mentoring, guidance, and support throughout my MD/PhD.

Partial results of this dissertation were previously published in the following journal articles:

A Fuchs G, Thevathasan T, Chretien YR, Mario J, Piriyapatsom A, Schmidt U, Eikermann M, Fintelmann FJ. **Lumbar Skeletal Muscle Index Derived from Routine Computed Tomography Exams Predict Adverse Post-Extubation Outcomes in Critically Ill Patients.** *Journal of Critical Care.* 2018;44:117-123.

B Nipp RD, Fuchs G, El-Jawahri A, Mario J, Troschel FM, Greer JA, Gallagher ER, Jackson VA, Kambadakone A, Hong TS, Temel JS, Fintelmann FJ. **Sarcopenia Is Associated with Quality of Life and Depression in Patients with Advanced Cancer.** *Oncologist.* 2018;23(1):97-104.

C Fuchs G, Chretien YR, Mario J, Do S, Eikermann M, Liu B, Yang K, Fintelmann FJ. **Quantifying the Effect of Slice Thickness, Intravenous Contrast and Tube Current on Muscle Segmentation: Implications for Body Composition Analysis.** *European Radiology.* 2018;28(6):2455-2463.

D Troschel AS, Troschel FM, Fuchs G, Marquardt JP, Ackman JB, Yang K, Fintelmann FJ. **Significance of Acquisition Parameters for Adipose Tissue Segmentation on CT Images.** *American Journal of Roentgenology.* 2021;217(1):177-185.

E Lee H, Troschel FM, Tajmir S, Fuchs G, Mario J, Fintelmann FJ, Do S. **Pixel-Level Deep Segmentation: Artificial Intelligence Quantifies Muscle on Computed Tomography for Body Morphometric Analysis.** *Journal of Digital Imaging.* 2017;30(4):487-498.

Table of Contents

List of figures

List of abbreviations

aIRR	Adjusted incidence rate ratios
aOR	Adjusted odds ratios
APACHE II	Acute Physiology and Chronic Health Evaluation II
B	Unstandardized coefficient beta
BMI	Body mass index
CCI	Charlson Comorbidity Index
CI	Confidence interval
CSA	Cross-sectional area
CT	Computed tomography
CTA	CT angiography
CV	Coefficient of variation
DSC	Dice similarity coefficient
ECOG	Eastern Cooperative Oncology Group
FACT-G	Functional Assessment of Cancer Therapy - General
FCN	Fully convolutional network
GPU	Graphics processing unit
HADS	Hospital Anxiety and Depression Scale
HIPAA	Health Insurance Portability and Accountability Act
HU	Hounsfield units
ICC	Intraclass correlation coefficient
ICD-9	International classification of diseases, 9th edition
ICU	Intensive care unit
IMAT	Intermuscular adipose tissue
IQR	Interquartile range
IRB	Institutional review board
IV	Intravenous
L3	Third lumbar vertebral body
L3SMI	L3 skeletal muscle index
LOS	Length of stay
M	Mean
mAs	Milliampere-second
MD	Mean difference

MGH	Massachusetts General Hospital
N	Population size
n	Sample size
p	P-value
PACS	Picture archiving and communication system
PET	Positron emission tomography
QoL	Quality of life
ROI	Region of interest
SAT	Subcutaneous adipose tissue
SD	Standard deviation
SE	Standard error
SMD	Skeletal muscle density
VAT	Visceral adipose tissue

Abstract

Objective: This thesis aims to evaluate the relationship between the skeletal muscle index derived from computed tomography (CT) images and patient outcomes, as well as its implications for patient care. This goal was pursued in five individual studies: Studies A and B evaluated the relationship between the lumbar skeletal muscle index (L3SMI) and patient outcomes in the intensive care unit (ICU) and oncology setting, respectively. Studies C and D evaluated the effect of CT acquisition parameters on body composition measures. Study E proposed a novel technique to automate the segmentation of skeletal muscle using a fully automated deep learning system.

Material and methods: In total, 1328 axial CT images were included in the five studies. Patients in studies A and B were part of the clinical trials NCT01967056 and NCT01401907 at Massachusetts General Hospital (MGH), respectively. Body composition indices were computed using semi-automated segmentation. Multivariable regression models with a priori defined covariates were used to analyze clinical outcomes. To evaluate whether CT acquisition parameters influence segmentation, the Bland-Altman approach was used. In study E, a fully convolutional neural network was implemented for deep learning-based automatic segmentation.

Results: Study A found lower L3SMI to be a predictor of increased mortality within 30 days of extubation ($p = 0.033$), increased rate of pneumonia within 30 days of extubation ($p = 0.002$), increased adverse discharge disposition ($p = 0.044$), longer hospital stays post-extubation ($p = 0.048$), and higher total hospital costs ($p = 0.043$). In study B, low L3SMI was associated with worse quality of life ($p = 0.048$) and increased depression symptoms ($p = 0.005$). Threshold-based segmentation of skeletal muscle in study C and adipose tissue compartments in study D were significantly affected by CT acquisition parameters. The proposed deep learning system in study E provided automatic segmentation of skeletal muscle cross-sectional area and achieved a high congruence to segmentations performed by domain experts (average Dice coefficient of 0.93).

Conclusion: L3SMI is a useful tool for the assessment of muscle mass in clinical practice. In critically ill patients, L3SMI can provide clinically useful information about patient outcomes at the time of extubation. Patients with advanced cancer who suffered from low muscle mass reported worse quality of life and increased depression symptoms. This highlights the clinical relevance of addressing muscle loss early on as part of a multimodal treatment plan. Importantly, indices utilized in body composition analysis are significantly affected by CT acquisition parameters. These effects should be considered when body composition analysis is used in clinical practice or research studies. Finally, our fully automated deep learning system enabled instantaneous segmentation of skeletal muscle.

Abstract in German

Zielsetzung: Das Ziel der vorliegenden Dissertation war es, den Einfluss des auf CT-Bildern berechneten Skelettmuskelindexes auf klinische Ergebnisse von Patienten und die daraus resultierenden Implikationen für die Patientenversorgung zu evaluieren. Dieses Ziel wurde in fünf Einzelstudien verfolgt: In den Studien A und B wurde der Einfluss des lumbalen Skelettmuskelindex (L3SMI) auf klinische Endpunkte von Patienten auf der Intensivstation sowie in der Onkologie untersucht. Die Studien C und D evaluierten die Auswirkungen von CT-Akquisitionsparametern auf Indizes der Körperzusammensetzung. Studie E stellte eine neuartige Technik der automatisierten Segmentierung von Skelettmuskulatur vor, die durch maschinelles Lernen ermöglicht wurde.

Material und Methoden: Insgesamt wurden 1328 axiale CT-Bilder in die fünf Studien eingeschlossen. Die Patienten der Studien A und B waren Teilnehmer der klinischen Studien NCT01967056 und NCT01401907 am Massachusetts General Hospital. Die Indizes der Körperzusammensetzung wurden mithilfe halbautomatischer Segmentierung berechnet. Die klinischen Endpunkte wurden in multivariablen Regressionsmodellen mit a priori definierten Kovariaten analysiert. Um zu evaluieren, ob CT-Akquisitionsparameter die Segmentierung beeinflussen, wurde der Bland-Altman-Ansatz verwendet. In Studie E wurden ein künstliches neuronales Netzwerk sowie maschinelles Lernen für die automatische Segmentierung eingesetzt.

Ergebnisse: In Studie A war ein niedriger L3SMI ein Prädiktor für eine höhere Mortalität ($p = 0.033$) und Pneumonierate ($p = 0.002$) innerhalb von 30 Tagen nach der Extubation sowie für mehr ungünstige Entlassungen ($p = 0.044$) und höhere Behandlungskosten für den gesamten Krankenhausaufenthalt ($p = 0.043$). Ein niedriger L3SMI war in Studie B mit einer schlechteren Lebensqualität ($p = 0.048$) und stärkeren depressiven Symptomen ($p = 0.005$) assoziiert. Die schwellenwertbasierte Segmentierung der Skelettmuskulatur in Studie C und der Fettgewebekompartimente in Studie D wurde durch CT-Akquisitionsparameter signifikant beeinflusst. Das in Studie E vorgestellte vollautomatische Segmentierungssystem erreichte eine hohe Übereinstimmung mit den durch Experten erstellten Segmentationen (durchschnittlicher Dice-Koeffizient von 0.93).

Fazit: Der L3SMI ist ein Werkzeug zur Beurteilung von Muskelmasse. Bei Intensivpatienten kann L3SMI zum Zeitpunkt der Extubation nützliche klinische Informationen liefern. Patienten mit fortgeschrittener Krebserkrankung, die zudem eine geringere Muskelmasse hatten, berichteten über eine schlechtere Lebensqualität und stärkere depressive Symptome. Dies unterstreicht die Notwendigkeit, die Muskulatur frühzeitig als Teil eines multimodalen Behandlungskonzeptes zu adressieren. Die Indizes der Körperzusammensetzung werden signifikant von CT-Akquisitionsparametern beeinflusst. Darüber hinaus ermöglichte unser vollautomatisiertes System dank maschinellen Lernens die verzögerungsfreie Segmentierung von Skelettmuskulatur.

Synopsis

1 Introduction

In medical imaging, the quantification of muscle mass has been demonstrated to correlate with a wide variety of relevant outcomes in clinical settings, including intensive care (1, 2), surgery (3, 4), and oncology (5, 6). There is a demand for an objective muscle assessment because clinical muscle assessments depend on the examiner's experience and patient cooperation, which can be affected by pain, restriction by medical devices, or communication barriers (7). Estimates of a patient's muscle reserves in routine care often rely on weight, bedside tests of muscle strength (7-9), or subjective judgment, which is referred to as the "eyeball test" by experienced clinicians (4). In contrast, body composition analysis based on medical imaging provides an objective assessment of muscle mass and does not rely on patient cooperation. Clinicians are often unaware of their patient's muscular resources based on routine clinical assessment (10). An international consensus highlighted the importance of evaluating sarcopenia (low muscle mass) on computed tomography (CT) imaging (11). Imaging data is readily available in various clinical settings, including surgery and oncology, as imaging protocols are integrated into routine clinical care (2, 12). Body composition analysis enables the extraction of clinically useful information from already-available medical imaging without additional costs or further radiation exposure. CT imaging is considered to be the gold standard for the quantification of muscle mass in body composition analysis (9, 12), and cadaver studies validated medical imaging as a reliable method of muscle measurement (13). Previous estimates of muscle mass on medical imaging often required multi-slice whole-body imaging and were therefore time-consuming and expensive. In search of a compromise between precision and cost, muscle cross-sectional area (CSA) at the level of the third lumbar vertebral body (L3) has been shown to correlate with whole-body muscle mass (14). Furthermore, muscle CSA measurements on CT were highly reproducible (2) and an objective technique to quantify muscle mass. By normalizing muscle CSA at L3 level for patients' statue (CSA divided by the square of patients' height), the resulting L3 skeletal muscle index (L3SMI) has been established as a surrogate marker for the muscle mass of patients (5, 6).

This doctoral thesis aimed to evaluate the relationship between skeletal muscle (represented by L3SMI) derived from CT images and patient outcomes as well as its implications for patient care. This aim was pursued in five published studies: studies A and B investigated the relationship between L3SMI and clinical outcomes in intensive care and oncology settings, studies C and D evaluated the effect of CT acquisition parameters on body composition indices, and study E explored the opportunity to automate the computation of L3SMI. Figure 1 provides a high-level overview of the studies conducted as part of this MD/PhD thesis.

Figure 1. High-level overview of the studies conducted as part of this thesis. CSA = cross-sectional area; CT = computed tomography; IV = intravenous; L3 = third lumbar vertebral body; L3SMI =L3 skeletal muscle index; SMD = skeletal muscle density.

First, we aimed to evaluate the relationship between L3SMI and patient outcomes in two studies in different clinical settings: intensive care (A) and oncology (B). Study A, including 231 patients from the intensive care unit (ICU), aimed to evaluate the relationship between CT-derived L3SMI and post-extubation outcomes in the ICU. In the intensive care setting, effective physiological ventilation is essential for successful extubation. Conventionally, it is presumed that lower muscle mass negatively impacts physiological ventilation (15), but the association between lean muscle mass and post-extubation outcomes has not previously been investigated. The hypothesis was that increased lean muscle mass is associated with lower 30-day mortality, decreased incidence of adverse discharge disposition, decreased incidence of pneumonia, and several secondary outcomes (16). Study B aimed to explore the relationship of L3SMI, quality of life (QoL), and mood in newly diagnosed patients with advanced cancer. In the face of an incurable disease, palliative care is often implemented to improve patients'

symptom burden and QoL. Although QoL and mood are suitable measures of the effectiveness of palliative care, data on the relationship between sarcopenia (objectively evaluated on CT images) and these patient-reported outcomes is missing. Investigating the relationship between sarcopenia and patients' mood and QoL might open up new opportunities to improve palliative care in patients with advanced cancer. A total of 237 oncology patients were included because sarcopenia is often present in patients with advanced cancer and adversely affects patient survival (5, 6) and physical function (17). The hypothesis was that a substantial share of patients with advanced cancer would fulfill the criteria for sarcopenia based on L3SMI measurements and that patients affected by sarcopenia would report worse mood and QoL symptoms (18).

Second, studies C and D aimed to evaluate the effect of imaging parameters on the obtained indices of body composition analysis. During the literature review, it became clear that previous studies rarely reported CT acquisition parameters of the analyzed scans. CT acquisition parameters affect image quality and can vary significantly between imaging protocols in clinical practice. Studies evaluating the effect of CT acquisition parameters on muscle segmentation were limited, and several influencing CT acquisition parameters had not been evaluated. Study C therefore aimed at quantifying the effect of CT acquisition parameters, including intravenous (IV) contrast, tube current, and slice thickness on the segmentation of skeletal muscle (19). This study, including 216 CT images, evaluated the effect of CT acquisition parameters on muscle CSA and skeletal muscle density (SMD). These two indices were chosen because they are frequently used in the body composition analysis of muscle. The mean attenuation of a computed CSA in Hounsfield units (HU) is defined as SMD, a measurement of muscular fat infiltration (20). CSA and SMD were calculated utilizing imaging software (OsiriX or 3D Slicer) which classifies pixels based on HU thresholds, a process known as image segmentation. Fixed thresholds are the current standard approach, using segmentation thresholds of -29 to +150 HU for muscle and -190 to -30 HU for fat (6, 13). Study D, including 244 CT images, aimed to evaluate the effect of CT acquisition parameters (IV contrast, tube current, tube potential, and slice thickness) on adipose tissue indices (21). Quantification and characterization of adipose tissue compartments is another emerging area of body composition analysis. Adipose tissue compartments include subcutaneous (SAT), visceral (VAT), and intermuscular adipose tissue (IMAT). Prior literature showed that SAT and VAT are associated with relevant clinical outcomes such as mortality (22, 23). Similar to the previously discussed topic of skeletal muscle segmentation, the effects of CT acquisition parameters on adipose tissue segmentation are incompletely understood. Therefore, we designed study D to evaluate the effect of CT acquisition parameters on adipose tissue segmentation.

Third, while working on the previous studies, the need for an efficient and reliable atomization tool for the segmentation of skeletal muscle became evident. Performing body composition analysis manually

on hundreds of CT examinations is time-consuming and carries a rater-dependent bias. Semi-automated threshold-based segmentation requires manual correction of segmentation errors based on visual analysis by domain experts. In order to establish body composition analysis as a clinical tool, automated segmentation systems are required, because they provide rapid and objective results. Adipose tissue segmentation can be reliably performed using a consistent HU range, but muscle segmentation is complicated by the potentially overlapping HU spectra of muscle and neighboring organs. Previously published automated segmentation strategies rely on experienced descriptive models of the appearance and shape of body compartments and cannot be generalized. Accurate differentiation between muscle tissue and adjunctive organs is challenging for traditional, intensity-based muscle segmentation algorithms due to their overlapping HU ranges. In contrast, data-driven approaches in machine learning have created a pathway for versatile, automated medical image segmentation applications. In study E, including CT images of 400 patients, we aimed to develop an automated deep learning system that enables fast and reliable muscle segmentation. This system could potentially facilitate the clinical application of body composition analysis across large patient populations (24). The neural network was trained to differentiate features between skeletal muscle and neighboring regions in order to achieve precise results. These approaches can be generalized because of their potential to learn distinguishing image features from raw data (25) instead of depending on descriptive models from domain experts.

2 Material and methods

Essential elements of the study designs and methodologies are outlined in this section. These aspects are presented in greater detail in the methods sections of the respective publications (16, 18, 19, 21, 24).

2.1 Study design

All studies conducted as part of this dissertation were HIPAA-compliant and approved by the institutional review board (IRB) of Massachusetts General Hospital (MGH) (16, 19, 21, 24) or the Dana-Farber Cancer Institute/ Harvard Cancer Center (18). Patient populations and study protocols were designed to tackle the particular research questions. Therefore, study protocols differed between the five studies and can be reviewed in detail in the respective publications (16, 18, 19, 21, 24).

Data from a prospective cohort study (NCT01967056) was utilized in the secondary analysis for study A. 231 adult patients were consecutively enrolled in two ICUs at the MGH. Patients who required intubation and mechanical ventilation were eligible for enrollment (16). As an example, figure 2 demonstrates the inclusion and exclusion criteria for study A.

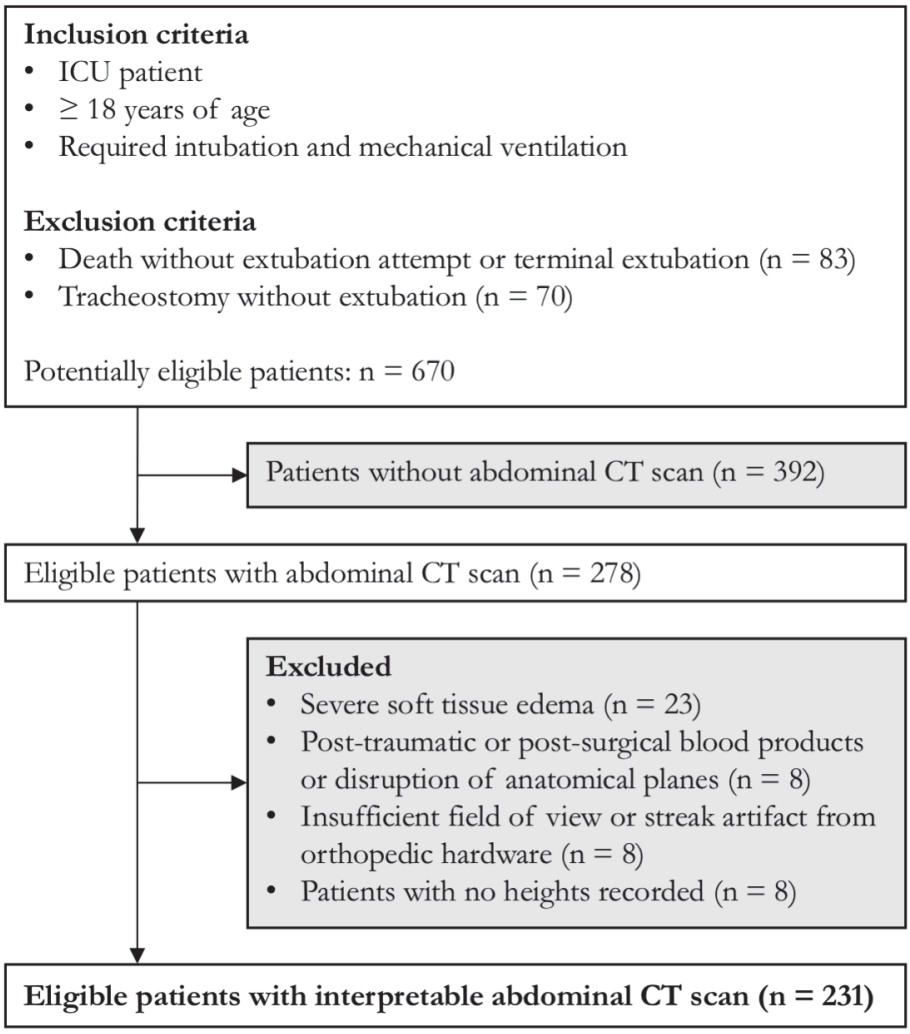

Figure 2. Inclusion and exclusion criteria for study A illustrated in a consort diagram. This figure was adapted from one of my previously published articles (16). ICU = intensive care unit; CT = computed tomography.

The study sample for study B comprised of 237 patients from the MGH Cancer Center who were approached within eight weeks after being diagnosed with incurable lung or non-colorectal gastrointestinal cancer. Patient-reported data were collected after informed consent, as part of a randomized clinical trial (NCT01401907) comparing early integrated palliative and oncology care versus oncology care alone (26).

For studies C and D, CT examinations were required that included at least two CT series of the same patient acquired within the same exam session. The departmental database (Department of Radiology at the MGH) was searched for CT examinations that included at least two series that were acquired using different CT acquisition parameters. In order to evaluate the effect of specific CT acquisition parameters, the series could only differ in the parameter that was investigated. A total of 216 images

in study C and 244 images in study D were included. Figure 3 illustrates the specific type of images chosen for these comparisons in study C (19).

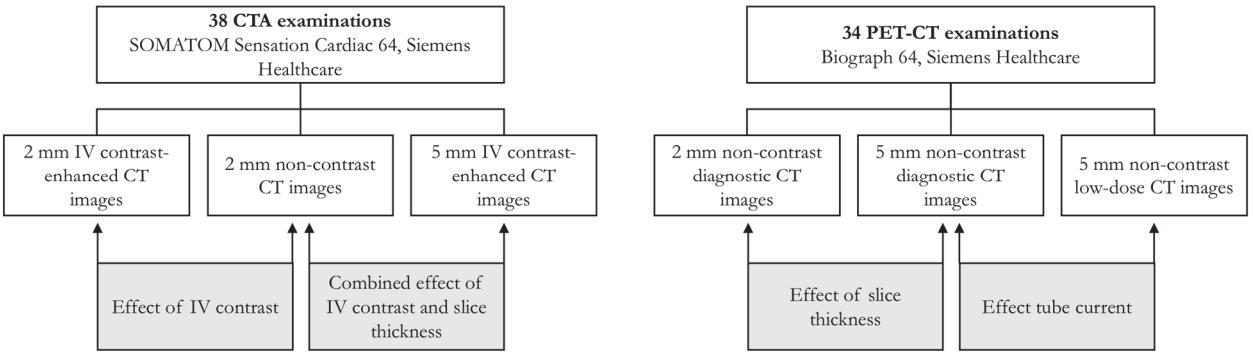

Figure 3. The two types of CT examinations that were used to investigate the effects of CT acquisition parameters on CT images. This figure was first published in one of my previous articles (19). Each CT examination comprised of three CT series that were acquired using different parameters. Two images of the same patient were compared (shaded boxes) that were obtained during the same examination (same time, same scanner). This allowed for appropriate analyses of the effects of CT acquisition parameters. CT = computed tomography; CTA = computed tomography angiography; IV = intravenous; PET = positron emission tomography.

The dataset for study E comprised of 400 CT examinations, including 200 female and 200 male patients. Patients were identified using an institutional database of lung cancer treatment at MGH. The treatment regimen required patients to undergo an abdominal CT scan with contrast, which was utilized in this study (24).

2.2 Image acquisition

All images were acquired on MGH CT scanners. Manufacturer-supplied phantoms were used for the daily calibration of CT scanners to ensure consistency with manufacturer recommendations. All images were acquired utilizing standardized departmental imaging protocols with patients in supine position. Detailed information on the scanner specifics and imaging protocols for each study is presented in the respective publications (16, 18, 19, 21, 24).

2.3 Image analysis

CT images were analyzed using open-source 3D Slicer (version 4.10.1; www.slicer.org) or OsiriX (version 7.0.2; Pixmeo, Bernex, Switzerland) software. Images were initially analyzed by the doctoral candidate (16, 18, 19) or another research assistant (21, 24) blinded to all clinical data and reviewed by a board-certified radiologist (minimum of 8 years of experience). All research assistants were trained by the radiologist to analyze radiological images and utilize the required image analysis tools. Exclusion

criteria were only met if the research assistant and the radiologist agreed that the muscle compartment could not be discriminated from the surrounding tissues. As an example, the exclusion criteria for study A are presented in figure 2. To evaluate inter- and intra-analyst agreement, the primary analyst and a second research assistant re-analyzed a random sample of 10 % of the CT images. The board-certified radiologist once again verified this reliability assessment.

All five studies utilized analyses of skeletal muscle CSA on a single axial image at the level of L3. CT images were identified and downloaded using the departmental picture archiving and communication system (PACS) and uploaded to OsiriX (16, 18, 19, 24) or 3D Slicer (21). The research database was managed on a departmental computer using OsiriX software connected to the departmental PACS server. Muscle CSA was measured using semi-automated, threshold-based segmentation with thresholds set at the standard HU range of -29 to +150 (6, 13). Based on anatomical landmarks, the analyst selected the regions of interest (ROIs) which contained muscle tissue. The threshold-based segmentation algorithm included in the OsiriX "Grow Region (2D/3D Segmentation)" software tool automatically segmented muscle compartments based on the defined HU thresholds. When necessary, the compartment boundaries were manually corrected prior to calculating CSA and mean attenuation. The "ExportROIs" plugin (an OsiriX software tool) was used to export numerical values for CSA and mean attenuation to STATA or SPSS software. A detailed manual on how to utilize the segmentation algorithm and the software tools, including a step-by-step guide, is available in my laboratory journal. Highlighted in figure 4 are the paraspinal, external and internal obliques, psoas, transversus abdominis, and rectus abdominis muscles, which are included in the calculated muscle CSA. The measured muscle cross-sectional area's mean attenuation (in HU) was defined as SMD, as previously described in the literature (20). For adipose tissue compartments, CSA and mean attenuation of SAT, VAT, and IMAT were computed similarly using semi-automated, threshold-based segmentation. For adipose tissue, thresholds of -190 HU to -30 HU were applied as previously described in the literature (13).

A **B**

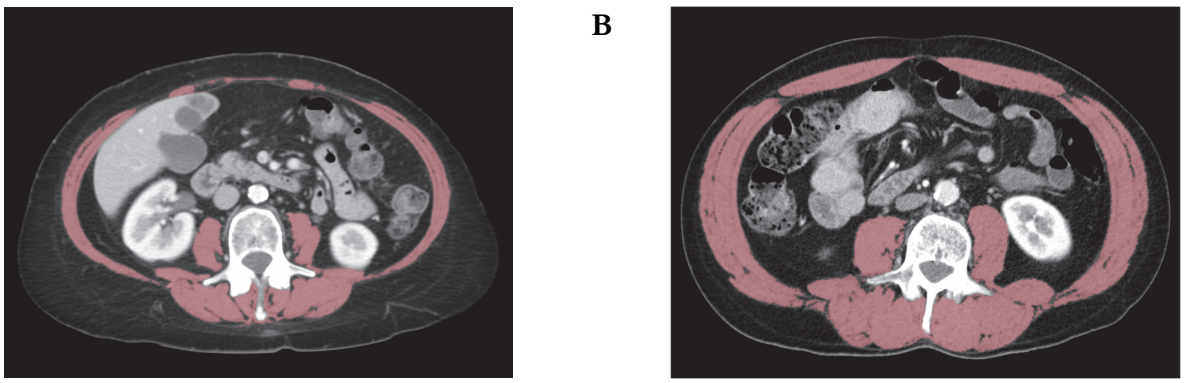

Figure 4. Axial images showing patients with low (**A**; 10th percentile) and high (**B**; 90th percentile) muscle mass. This figure was first published in one of my previous articles (18). The CT images are presented at the level of L3, with muscle CSA highlighted in red. CSA of paraspinal, external and

internal obliques, psoas, transversus abdominis, and rectus abdominis muscles was calculated using semi-automated threshold-based segmentation. **A**: Image of a 61-year-old female patient with a L3SMI of 34.2 cm^2/m^2. **B**: Image of a 53-year-old male patient with a L3SMI of 60.4 cm^2/m^2. CSA = cross-sectional area; CT = computed tomography; L3 =third lumbar vertebral body; L3SMI = L3 skeletal muscle index.

2.4 Clinical data

Clinical data for study A were collected from medical records and study documents. Data comprised age, body mass index (BMI), gender, height, hospital length of stay (LOS), post-extubation and total ICU LOS, mortality within 30 days post-extubation, past medical history, re-intubation within 72 h post-extubation, Acute Physiology and Chronic Health Evaluation (APACHE) II score on ICU admission, and Charlson Comorbidity Index (CCI). Acute respiratory failure, atelectasis, pneumonia, and pulmonary edema within 30 days post-extubation were defined based on the international classification of diseases, 9th edition (ICD-9) diagnosis codes. Data on total hospital costs and discharge destination were extracted through Enterprise Performance Systems Inc. software (Allscripts Healthcare, Chesterfield, USA). The sum of direct (fixed and variable costs) and indirect costs (fixed costs assigned in a step-down structure to respective departments) associated with patient services is presented as total hospital costs. Total hospital costs represent estimates of what MGH senior management believes to be the "true" costs of care at MGH. The outcome "adverse discharge disposition" is based on the primary discharge destination from the MGH. Discharges to a skilled nursing facility, a swing bed provider, a long-term care facility, or the occurrence of in-hospital mortality were defined as adverse. Other discharge destinations were defined as non-adverse (27).

Clinical data for study B were collected from medical records, a demographic questionnaire, and assessments which participants completed as part of the study protocol at baseline. Data from medical records included age, cancer diagnosis, initial cancer treatment, Eastern Cooperative Oncology Group (ECOG) performance status, and sex. A patient questionnaire was used to capture the patient's education, ethnicity, income, race, relationship status, religion, and smoking history. Functional Assessment of Cancer Therapy - General (FACT-G) was used to assess patients' QoL (28). A total of 27 items, applying a five-point Likert scale ranging from 0 (not at all) to 4 (very much), are utilized as part of the FACT-G to assess patients' well-being across four domains (emotional, functional, physical, and social). Higher scores suggest a better QoL. The Hospital Anxiety and Depression Scale (HADS) monitored patients' anxiety and depression symptoms (29). The 14-item HADS comprises two seven-item subscales, both with a score range of 0 to 21, aimed at assessing anxiety and depression symptoms, with higher scores indicating worse symptoms.

2.5 Statistical analysis

Descriptive statistics, such as frequencies, means, medians, interquartile range (IQR), and standard deviations (*SDs*) were used to analyze the clinical data. Statistical testing was two-tailed, and the statistical significance level was defined as $p \leq 0.05$. To investigate whether radiological markers independently correlate with clinical outcomes, multivariable linear regression models were built for continuous outcomes, and multivariable logistic regression models were built for categorical outcomes. Independent variables were defined a priori based on the respective literature and their importance for clinical care to prevent falsely identifying significant results. Results of the multivariable models are reported as adjusted incidence rate ratios (aIRRs) or adjusted odds ratios (aORs) with 95 % confidence intervals (*CI*s) and *p*-values. Predicted probabilities derived from multivariable logistic regression models were used to illustrate the effect of radiological markers on dichotomous outcomes across a spectrum of possible values. Independent samples Student's *t*-test for continuous variables, and Wilcoxon sign-ranked test (21) or Fisher's exact test (18) for categorical variables were used as appropriate to compare study samples. The effects of CT acquisition parameters on CSA and mean attenuation measurements were assessed using the Bland-Altman approach (30). For the Bland-Altman analysis, CSA and mean attenuation values were computed from CT examinations that included at least two series that were acquired using different CT acquisition parameters. These series of the same patient were obtained during the same examination on the same scanner. Therefore, differences between series of that examination were attributed to the change in specific CT acquisition parameters (figure 3). The Shapiro-Wilk (21) or the Kolmogorov-Smirnov (19) normality test showed that differences in muscle measurements were normally distributed. Within-subject coefficients of variation (CVs) and two-way mixed-effects intraclass correlation coefficients (ICCs) were used to evaluate intra- and inter-analyst agreement of the image analysis. The level of agreement was based on the congruence of segmented regions. SPSS version 25.0 (IBM, Armonk, NY) or STATA version 13.0 (StataCorp, College Station, USA) software was used to perform the statistical analyses.

2.6 Utilization of a fully automated deep learning system

A fully automated, deep learning-based tool for skeletal muscle segmentation on axial CT images is proposed in study E (24). The proposed segmentation pipeline is outlined in figure 5 and described in technical detail in the paper (24). In brief, a dataset of 400 CT images paired with their manual segmentation was used for training a fully convolutional network (FCN). The proposed system enables instantaneous segmentation of skeletal muscle.

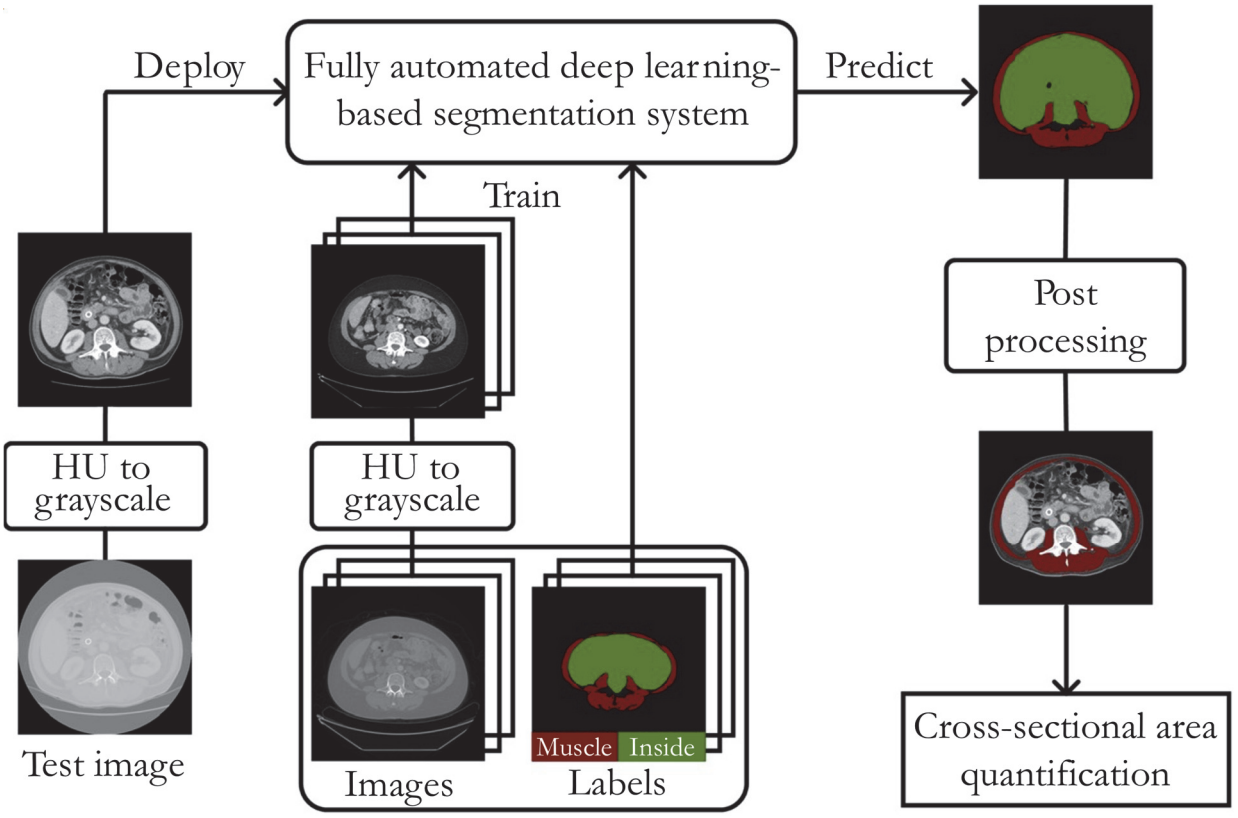

Figure 5. A high-level overview of the fully automated deep learning-based segmentation system for skeletal muscle on axial CT images. This figure was adapted from one of my previously published articles (24). Axial CT images at the L3 level are processed using a fully convolutional network approach, including grayscale image conversion followed by post-processing. CT = computed tomography; HU = Hounsfield units; L3 = third lumbar vertebral body.

Domain experts manually created muscle segmentation masks in OsiriX software to train the system. Axial images connected to their corresponding segmentation maps were reformatted to serve as input for the FCNs. Out of the 400 patients included in this study, images of 150 patients were withheld for subsequent system testing. This subset, which was used for validation, comprised randomly selected images of 25 female and 25 male patients from each weight group (normal weight, overweight, and obese). The remaining images of 250 patients were used to train the FCNs. All evaluated systems were trained for a period of approximately 500 epochs. Deep neural networks are typically trained for multiple epochs. An epoch, in the context of machine learning, is one complete pass of the training data. All computations were performed on a developer machine (DevBox, NVIDIA Corp, Santa Clara, CA) holding four TITAN X graphics processing units (GPUs) with 12 gigabytes of memory per GPU using Nvidia DIGITS (version 5.1) and Nvidia-Caffe (version 0.15.14). The degree of overlap between the semi-automated segmentation mask approved by the radiologist and the FCN-derived mask was evaluated across five FCN architectures. These models of increasing granularity (FCN-32s, FCN-16s, FCN-8s, FCN-4s, and FCN-2s) were assessed using the held-out subset of 150 patient images to

determine the best performing FCN. Dice similarity coefficient (DSC), a metric for congruence of two binary segmentation results, and CSA error were calculated to evaluate the segmentation quality. Please see study E for the detailed equations (24). This work was realized in collaboration with the MGH Laboratory of Medical Imaging and Computation. A detailed technical description of the training process and system evaluation is provided in study E (24). This thesis primarily describes the radiological image analysis and its implications for clinical practice.

3 Results

This section provides an overarching summary of the key results. Further information on additional outcomes is presented in the respective sections of the five published articles (16, 18, 19, 21, 24). A total of 1328 axial images at the L3 level were selected from routine CT examinations and included in the studies conducted as part of this MD/PhD thesis. For the analysis of muscle CSA, the inter-analyst agreement was excellent, with ICC values ranging from 0.985 to 0.999 in the studies. Intra-analyst agreement analysis also showed excellent ICC values, ranging from 0.996 to 1.000 in the studies.

3.1 Associations of skeletal muscle index and clinical outcome

In the two clinical studies, a higher skeletal muscle index was associated with improved clinical outcomes in the ICU as well as the oncology setting. The results of studies A and B are presented in the two following subsections.

3.1.1 Associations of skeletal muscle index and post-extubation outcomes in the intensive care setting

The ICU study population in study A was comprised of N = 231 patients from various diagnostic categories, including non-surgical (25.5 %), emergency surgery (31.6 %), surgery after trauma (20 %), and elective surgery (22.9 %).

Mortality at 30 days post-extubation was 6.5 % (n = 15). Figure 6 illustrates the significant difference between the deceased patients and the remaining study population at 30 days post-extubation, respectively (mean [M] = 46.9 cm^2/m^2 [SD ± 10.7] vs. M = 58.5 cm^2/m^2 [SD ± 15.3]; p = 0.005). The multivariable logistic regression analysis found L3SMI to be a predictor for 30-day mortality (aOR = 0.94; 95 %-CI = [0.890–0.995]; p = 0.033).

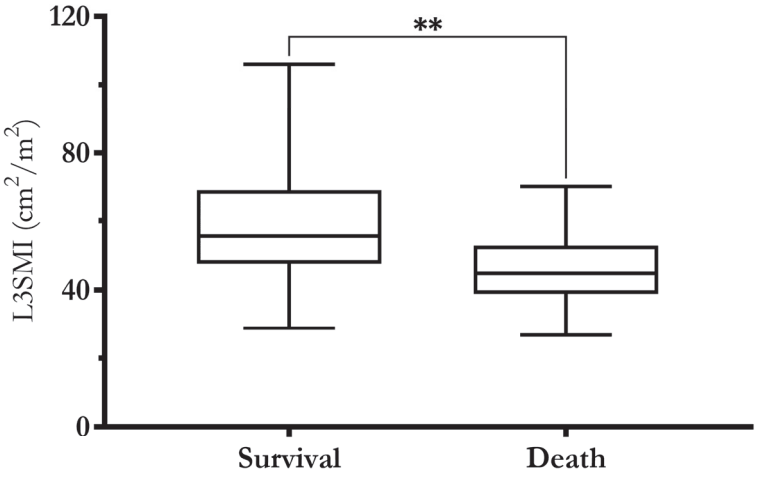

Figure 6. Box plot illustrating the distribution and difference of L3SMI values between patients who were deceased (death) or alive (survival) at 30 days after extubation. This figure was first published in one of my previous articles (16). Asterisks (**) indicate a *p*-value < 0.01, two-sample *t*-test (p = 0.005). L3SMI = L3 skeletal muscle index.

Adverse discharge after extubation occurred in 33.3 % (n = 77) of patients. In a multivariable logistic regression analysis, L3SMI predicted adverse discharge (aOR = 0.98; 95 %-*CI* = [0.957–0.999]; p = 0.044). Mean predicted probabilities which were derived from the multivariable logistic regression model are displayed in figure 7. The covariates age, CCI, and APACHE II score were set at their medians for illustrative purposes. The model estimated a 45.1 % probability of adverse discharge disposition for a 60-year-old patient with an L3SMI of 35 cm^2/m^2, CCI of 1, and APACHE II score of 16. For a ten-unit increase in L3SMI (from 35 to 45 cm^2/m^2), the model estimated a 5.5 % decreased likelihood of adverse discharge.

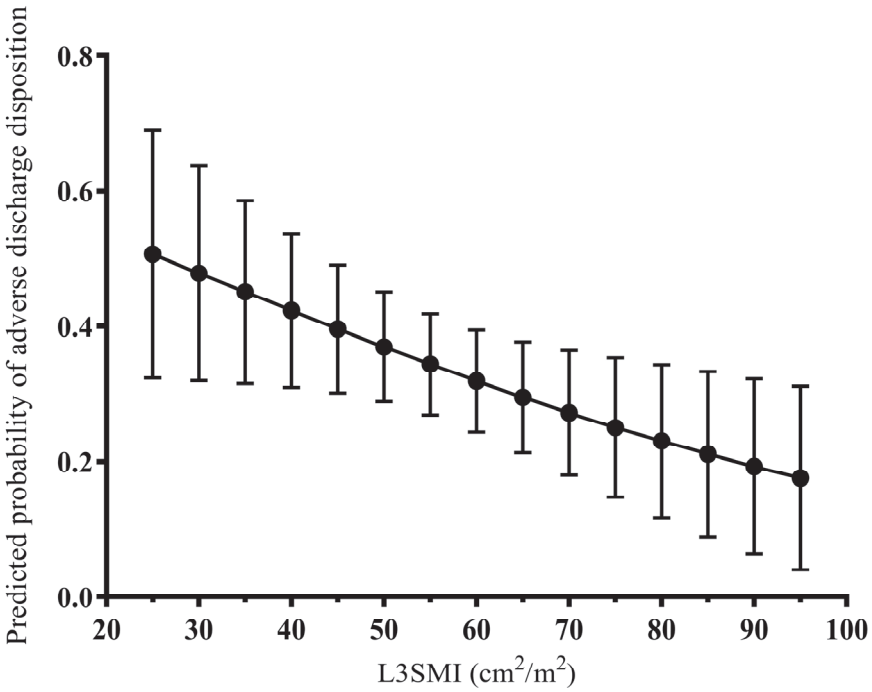

Figure 7. Mean predicted probabilities of adverse discharge disposition illustrated as a function of L3SMI including 95 % confidence intervals. This figure was first published in one of my previous articles (16). Covariates of the multivariable logistic regression model were set at their medians for illustrative purposes (age = 60 years, Charlson Comorbidity Index = 1, Acute Physiology and Chronic Health Evaluation II score = 16). L3SMI = L3 skeletal muscle index.

Of the ICU-patients, 32.5 % (n = 75) had a pneumonia diagnosis within 30 days of extubation. In the multivariable logistic regression model, L3SMI predicted pneumonia (aOR 0.96; 95 %-*CI* = [0.941,0.986]; p = 0.002). The model estimated a 49.5 % probability of acquiring pneumonia for a 60-year-old patient with an L3SMI of 35 cm^2/m^2, CCI of 1, and APACHE II score of 16. For a ten-unit increase in L3SMI (from 35 to 45 cm^2/m^2), the model estimated a 9.3 % decreased likelihood of acquiring pneumonia within 30 days of extubation.

Within 72 hours of extubation, 11.7 % of patients (n = 27) were reintubated. L3SMI values were significantly lower for patients who were reintubated than for patients that were not (M = 51.47 cm^2/m^2 [SD ± 13.20] vs. M = 58.53 cm^2/m^2 [SD ±15.40]; p = 0.024). Increased L3SMI predicted shorter hospital LOS after extubation (aIRR 0.99; 95 %-*CI* = [0.986, 1.000]; p = 0.048) with the average hospital LOS post-extubation being 19.3 days (SD ± 18.3). In a multivariable ordered logistic regression model with total hospital costs divided into quartiles, L3SMI predicted total hospital costs (aOR 0.98; 95 %-*CI* = [0.966, 0.999]; p = 0.043) (16).

3.1.2 Associations of skeletal muscle index and patient-reported measures in the oncology setting

Within the oncologic study population included in study B (N = 237), L3SMI was used to differentiate between patients with and without sarcopenia. Based on the sarcopenia definition by the international consensus for cancer cachexia (L3SMI of < 39 cm^2/m^2 for women and < 55 cm^2/m^2 for men) (31), 55.3 % (n = 131) of patients in study B were sarcopenic. Linear multivariable regression models were used to evaluate the association between sarcopenia and patient-reported measures. The models were adjusted for patients' age, cancer type, sex, education, and marital status.

The regression model showed an association between sarcopenia and worse QoL, as indicated by decreased FACT-G scores (unstandardized coefficient beta [B] = -4.26, standard error [SE] = 2.15, 95 %-CI = [-8.49, 0.03], p = 0.048). Increased rates of clinically significant depression symptoms (29.0 % vs. 16.0 %, p = 0.021) were also found in the sarcopenic patient population. Sarcopenia was independently associated with increased HADS-depression scores in the multivariable linear regression model (B = 1.56, SE = 0.55, 95 %-CI = [0.47, 2.65], p = 0.005) (18).

3.2 Effect of CT acquisition parameters on body composition analysis

The CT acquisition parameters (IV contrast, tube current, tube potential, and slice thickness) significantly affected the computation of tissue compartments on CT images. The results of studies C and D are presented in the two following subsections.

3.2.1 Effect of CT acquisition parameters on semi-automated threshold-based segmentation of skeletal muscle

IV contrast, tube current, and slice thickness significantly affected the computation of skeletal muscle in study C (19). Figure 8 illustrates the effects of each CT acquisition parameter utilizing graphs that highlight the changes within the CT image's pixel distribution between HU values.

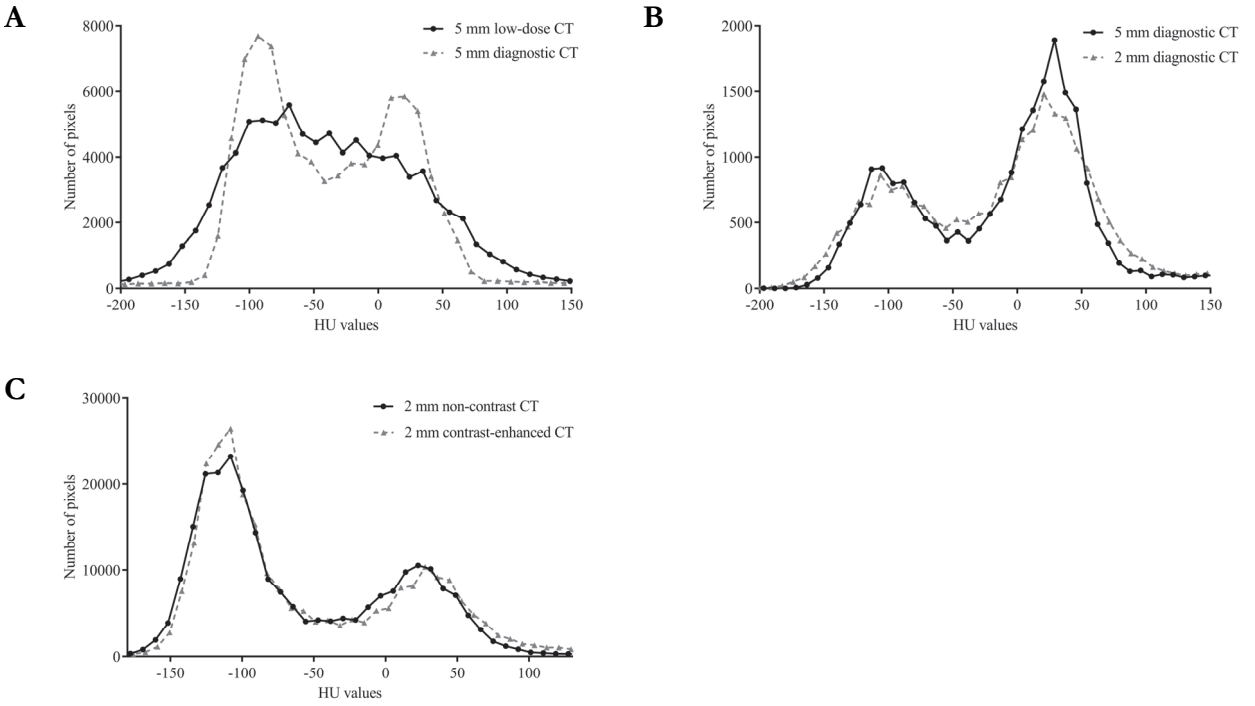

Figure 8. Effect of CT acquisition parameters on the distribution of pixels between Hounsfield unit (HU) values. This figure was first published in one of my previous articles (19). The lines between data-points facilitate the visual differentiation between the two different scenarios of CT acquisition parameters per graph. Plot **A** illustrates the histograms of 5 mm low-dose and 5 mm diagnostic CT images. Less articulated spectral peaks and increased histogram spread can be observed in the low-dose image compared to the diagnostic image. This can be explained by higher noise within the CT image resulting in less differentiation between the two peaks of the histogram. Plot **B** shows the histograms of 5 mm diagnostic and 2 mm diagnostic CT images. Only subtle but significant ($p < 0.0001$) differences (shallower peaks and slightly elevated valleys) can be observed between the histograms. Compared to the 5 mm CT image, the increased spread of the histogram indicates slightly higher noise within the 2 mm CT image. Plot **C** displays the histograms of 2 mm non-contrast and 2 mm IV contrast-enhanced CT images. The presence of IV contrast results in a slight rightward shift (and therefore greater HU values) of the histogram for the IV contrast-enhanced image.

The tube current had a significant effect on the computation of CSA as well as SMD values on CT images. CSA values were significantly smaller when calculated on 5 mm low-dose CT images (average -4.8 %) compared to 5 mm diagnostic CT images (Mean difference [*MD*] = -6.44 cm^2; 95 %-*CI* = [-9.10, -3.78]; $p < 0.0001$). SMD values were significantly greater when computed on 5 mm low-dose images (average +46.5 %) compared to 5 mm diagnostic CT images (*MD* = 8.10 HU; 95 %-*CI* = [6.48, 9.71] HU; $p < 0.0001$).

Varying slice thickness affected the computation of CSA values less than that of SMD values. CSA values were significantly greater when computed on 5 mm CT images (average +1.1 %) compared to 2 mm CT images (*MD* = 1.32 cm^2; 95 %-*CI* = [0.78, 1.85]; $p < 0.0001$). SMD values were significantly

smaller when calculated on 5 mm CT images (average -11.6 %) compared to 2 mm CT images (*MD* = -2.36 HU; 95 %-*CI* = [-2.79, -1.94]; $p < 0.0001$).

The effect of intravenous contrast on calculated CSA as well as SMD values was significant. CSA values were significantly greater when computed on IV contrast-enhanced CT images (average +1.9 %) compared to non-contrast CT images (*MD* = 2.33 cm^2; 95 %-*CI* = [1.76, 2.89]; $p < 0.0001$). SMD values were significantly greater on IV contrast-enhanced CT images (average +6,0 %) compared to those computed on non-contrast CT images (*MD* = 1.35 HU; 95 %-*CI* = [0.79, 1.91]; $p < 0.0001$).

3.2.2 Effect of CT acquisition parameters on semi-automated threshold-based segmentation of adipose tissue compartments

In study D, the tube potential significantly affected CSA of all three adipose tissue compartments (SAT, VAT, and IMAT). Computed CSA values for higher tube potential were decreased for SAT (-4.2 %, $p < 0.001$) as well as VAT (-2.8 %, $p = 0.001$), but increased for IMAT (+5.4 %, $p = 0.001$). For higher tube potential mean attenuation values were increased in all compartments (+20.8 % for SAT, $p < 0.001$; +11.7 % for VAT, $p < 0.001$; +6.2 % for IMAT, $p < 0.001$).

Lower effective milliampere-second (mAs) affected CSA in all adipose tissue compartments (-3.2 % for SAT, $p < 0.001$; -12.6 % for VAT, $p = 0.001$; +58.8 % for IMAT, $p < 0.001$). For all three compartments, mean attenuation was reduced on low-dose images (-1.8% for SAT, $p < 0.001$; -3.6 % for VAT, $p < 0.001$; -8.7 % for IMAT, $p < 0.001$).

Thinner slice thickness significantly increased the computed CSA values for VAT (+3.0 %, $p = 0.005$) and IMAT (+17.3 %, $p < 0.001$). The CSA values for SAT were less affected (-0.2 %, $p = 0.851$). For thinner slices, mean attenuation values were significantly decreased in all three compartments (-1.0 % for SAT, $p < 0.001$; -2.4 % for VAT, $p < 0.001$; -5.4 % for IMAT, $p < 0.001$).

Presence of IV contrast significantly decreased CSA values of SAT (-0.4 %, $p = 0.029$) and IMAT (-9.3 %, $p < 0.001$). The CSA for VAT was also decreased (-2.0 %, $p = 0.131$). In all three compartments, mean attenuation values were increased significantly (+0.8 % for SAT, $p < 0.001$; +1.7 % for VAT, $p < 0.001$; +0.8 % for IMAT, $p = 0.03$) (21). Figure 9 illustrates the effect of CT acquisition parameters which were investigated in study D.

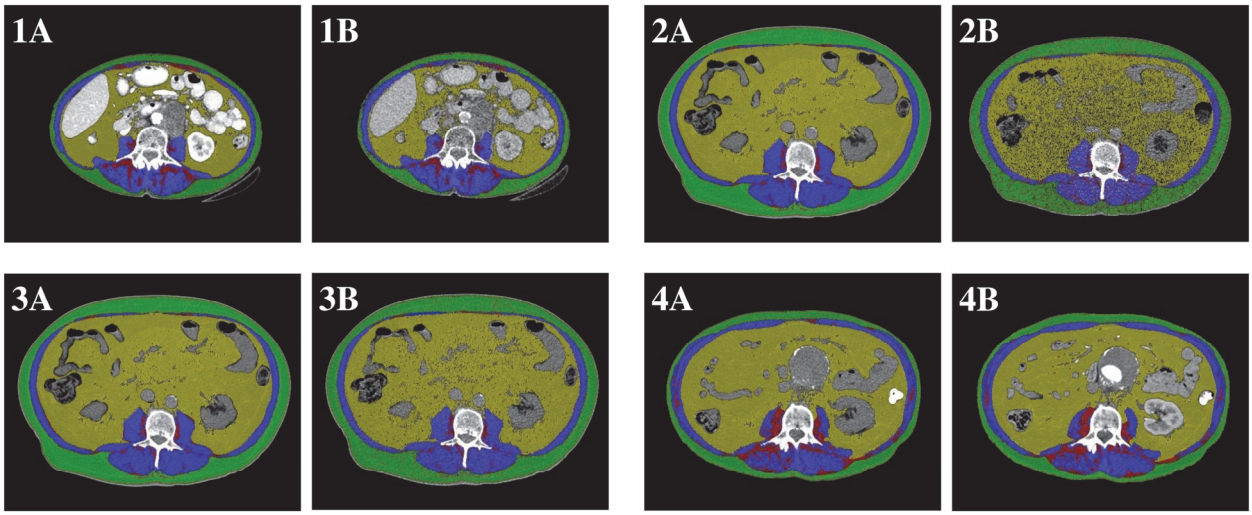

Figure 9. CT acquisition parameters' effect on segmentation outputs of adipose tissue compartments. This figure was adapted from one of my previously published articles (21), and was presented at the RSNA annual meeting 2019. Axial CT image pairs of the same patient were obtained during the same examination (same time, same scanner). Each CT examination included at least two series that were acquired using different CT acquisition parameters. Illustrated are the effects of tube potential (100 kVp [**1A**] vs. 150 kVp [**1B**]), tube current (diagnostic quality [**2A**] vs. low dose CT image [**2B**]), slice thickness (5 mm [**3A**] vs. 2 mm thick CT slices [**3B**]) and IV contrast (non-contrast [**4A**] vs. contrast-enhanced CT image [**4B**]). Green = subcutaneous adipose tissue (SAT); yellow = visceral adipose tissue (VAT); red = intermuscular adipose tissue (IMAT); blue = skeletal muscle.

3.3 Fully automated deep learning system for the segmentation of skeletal muscle

In study E, the performance of five trained FCN models with different architectures was compared to manually created segmentation masks approved by a board-certified radiologist (minimum of 8 years of experience). The most fine-grained FCN-2s model achieved an average CSA error of 3.68 % (*SD* ± 2.29) and an average DSC of 0.93 (*SD* ± 0.02). Compared to the most coarse-grained FCN model, this represents an 80 % decrease in CSA error and a 59 % improvement in DSC. The best performing FCN-2s model achieved excellent agreement with manually segmented images, as illustrated in figure 10. Even though the errors were small in relation to the overall CSA, the three main errors were incomplete muscle segmentation (n = 58; 38.7 % of test cases), incorrect organ segmentation (n = 52; 34.7 % of test cases), and subcutaneous edema mischaracterized as muscle (n = 17; 11.3 % of test cases). In obese patients, the incorrect characterization of subcutaneous soft tissue edema as muscle CSA was significantly more common compared to non-obese patients (p = 0.018). The complete segmentation of the 150-patient subset took 25 seconds on average (0.17 seconds per CT image), performed by utilizing a single TITAN X GPU. Manual segmentation of these 150 images would take approximately 50 working hours. On average, the creation of the segmentation mask by domain experts plus the subsequent evaluation by the consultant radiologist required approximately 20 minutes per CT image.

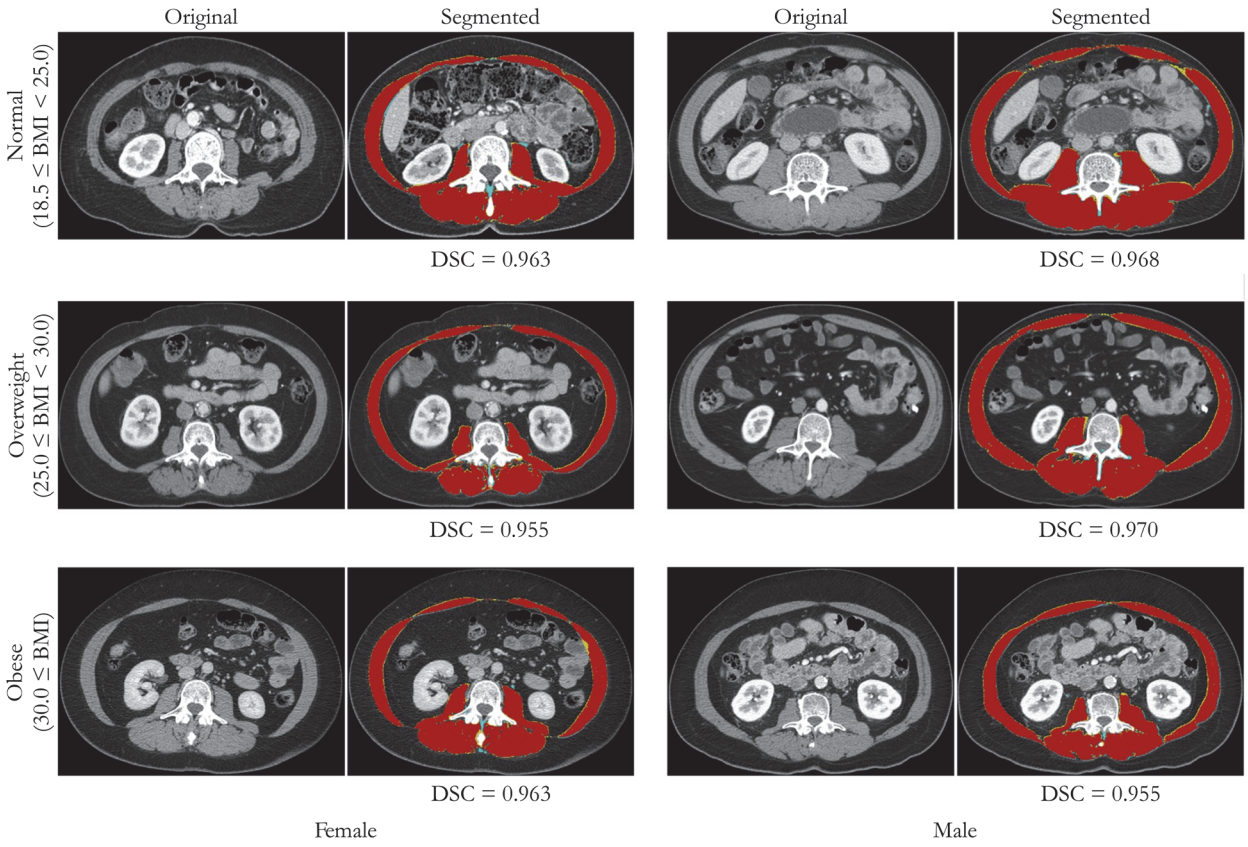

Figure 10. Six examples of muscle segmentation masks created by the fully automated deep segmentation system compared to manual segmentation maps. This figure was adapted from one of my previously published articles (24). One CT image from every category (weight and gender) is presented, including its segmentation mask next to the original axial CT image. The Dice similarity coefficient (DSC) is indicated below each image, which was segmented by the fully convolutional network FCN-2s. Compared to the manually segmented image, areas over-sampled by the FCN-2s are highlighted in blue, under-sampled areas are highlighted in yellow, and correctly segmented areas are highlighted in red.

4 Discussion

4.1 Overarching summary

The five studies add to the growing body of literature that establishes body composition analysis as a useful tool for the assessment of muscle mass in clinical practice. This doctoral thesis evaluates the relationship between skeletal muscle measurements and patient outcomes and its implications for patient care. Studies A and B evaluated associations of L3SMI and clinical outcomes in two different clinical settings. In the ICU setting in study A, the muscle mass surrogate L3SMI predicted a variety of important clinical outcomes in adult ICU patients. Measurement of this muscle index can be reliably computed from routine abdominal CT images. The covariates CCI and APACHE II score were selected to control for underlying comorbidities and acute illnesses. Lower L3SMI was a predictor of increased mortality within 30 days of extubation ($p = 0.033$), increased rate of pneumonia within 30 days of extubation ($p = 0.002$), increased adverse discharge disposition ($p = 0.044$), longer hospital LOS post-extubation ($p = 0.048$), and higher total hospital costs ($p = 0.043$). The univariable analysis also revealed that patients who were reintubated within 72 hours after extubation had a significantly lower L3SMI than patients who did not require reintubation ($p = 0.024$). Study A demonstrated that L3SMI could be utilized as a prognostic tool in an adult ICU population at the time of extubation (16).

Study B showed in the oncology setting that sarcopenia is highly prevalent among patients with recently diagnosed, advanced lung and gastrointestinal cancer. In this study, L3SMI thresholds were used for the definition of sarcopenia as suggested by the international consensus for cancer cachexia (31). Based on this definition, more than half of the patient sample met the criteria for sarcopenia. Sarcopenia was associated with increased depression symptoms and worse QoL. Specifically, sarcopenia was associated with decreased FACT-G scores ($p = 0.048$) and increased HADS-depression scores ($p = 0.005$) (18). These findings suggest that addressing sarcopenia early on as part of the treatment plan for patients with advanced cancer could improve patients' quality of life and mood. However, this relationship is not necessarily causal and needs to be explored more thoroughly.

As a next step, we aimed to further evaluate the validity of indices used in body composition analysis. Studies C and D therefore systematically evaluated the effect of modifiable CT acquisition parameters on the threshold-based segmentation used for body composition analysis. By modifying only one CT acquisition parameter at a time and keeping all other factors constant, the studies managed to quantify the effect of individual CT acquisition parameters. Study C showed that IV contrast ($p < 0.0001$), slice thickness ($p < 0.0001$), and tube current ($p < 0.0001$) significantly affect threshold-based segmentation of skeletal muscle CSA and SMD (19). Study D analyzed the effect of CT acquisition parameters on

the threshold-based segmentation of adipose tissue compartments. It showed that IV contrast, tube current, tube potential, and slice thickness significantly affect the computation of CSA and mean attenuation of adipose tissue in SAT, VAT, and IMAT (21). The two studies suggested that the effects of CT acquisition parameters on threshold-based segmentation should be taken into account when body composition analysis is used in clinical practice or research studies.

Finally, in study E, we propose a fully automated, deep-learning-based tool for skeletal muscle segmentation on axial CT images. Due to overlapping HU ranges, traditional, intensity-based muscle segmentation algorithms often fail to distinguish muscle from the neighboring tissues. By training a fully convolutional network with the manual segmentation maps obtained previously, this method was able to mimic the segmentation quality of experts for every new image. An average DSC of 0.93 (*SD* ± 0.02) and CSA error of 3.68 % (*SD* ± 2.29) indicated excellent agreement with manually segmented images. By intrinsically learning characteristics of skeletal muscle, this processing pipeline enabled instantaneous segmentation of large datasets. It is also a shareable tool for other researchers. Compared to the time-consuming semi-automated threshold-based segmentation, the deployment time was greatly accelerated from about 20 minutes to 0.17 seconds per CT image analysis. An overview of the findings presented in the five respective publications is provided in figure 11.

1 Associations of skeletal muscle index and clinical outcome

Study A: Lumbar Skeletal Muscle Index Derived from Routine Computed Tomography Exams Predict Adverse Post-Extubation Outcomes in Critically Ill Patients

- *Objective:* To evaluate the effect of L3SMI on patient outcomes in the intensive care unit.
- *Hypothesis:* Increased L3SMI is associated with better clinical outcomes in the intensive care unit.
- *Results:* Lower L3SMI was a predictor of increased mortality within 30 days of extubation ($p = 0.033$), increased rate of pneumonia within 30 days of extubation ($p = 0.002$), increased adverse discharge disposition ($p = 0.044$), longer hospital stays post-extubation ($p = 0.048$), and higher total hospital costs ($p = 0.043$).
- *Conclusion:* L3SMI is a useful prognostic tool at the time of extubation.

Study B: Sarcopenia Is Associated with Quality of Life and Depression in Patients with Advanced Cancer

- *Objective:* To investigate the associations between sarcopenia and patients' quality of life and mood.
- *Hypothesis:* A substantial proportion of patients with advanced cancer meet criteria for sarcopenia on CT images and these patients report worse quality of life and mood symptoms.
- *Results:* 55 % of patients met the criteria for sarcopenia on CT images. Sarcopenia was associated with lower FACT-G scores ($p = 0.048$) and higher HADS-depression scores ($p = 0.005$).
- *Conclusion:* Sarcopenia was highly prevalent among patients with advanced cancer and these patients experienced worse quality of life and depression symptoms.

2 Effect of CT acquisition parameters on body composition analysis

Study C: Quantifying the Effect of Slice Thickness, Intravenous Contrast and Tube Current on Muscle Segmentation: Implications for Body Composition Analysis

- *Objective:* To investigate the effect of IV contrast, tube current, and slice thickness on threshold-based segmentation of skeletal muscle CSA and SMD on routine CT.
- *Hypothesis:* CT acquisition parameters significantly affect the segmentation of skeletal muscle CSA and SMD.
- *Results:* Segmentation of CSA as well as SMD was significantly influenced by changes of IV contrast ($p < 0.0001$), tube current ($p < 0.0001$) and slice thickness ($p < 0.0001$). Inter- and intra-analyst agreement was excellent.
- *Conclusion:* IV contrast, tube current and slice thickness significantly influence threshold-segmentation of CSA and SMD on routine CT.

Study D: Significance of Acquisition Parameters for Adipose Tissue Segmentation on CT Images

- *Objective:* To investigate the effect of IV contrast, tube current, tube potential and slice thickness on threshold-based segmentation of CSA and mean attenuation of adipose tissue compartments.
- *Hypothesis:* CT acquisition parameters have a significant effect on the segmentation of adipose tissue CSA and mean attenuation.
- *Results:* Changes in IV contrast, tube current, tube potential and slice thickness significantly influenced the segmentation of CSA and mean attenuation of the adipose tissue compartments SAT, VAT and IMAT.
- *Conclusion:* IV contrast, tube current, tube potential, and slice thickness significantly influence threshold-based segmentation of CSA and mean attenuation of adipose tissue compartments.

3 Fully automated deep learning system for the segmentation of skeletal muscle

Study E: Pixel-Level Deep Segmentation: Artificial Intelligence Quantifies Muscle on Computed Tomography for Body Morphometric Analysis

- *Objective:* To develop a fully automated deep learning system for the segmentation of skeletal muscle CSA on axial CT images.
- *Hypothesis:* The segmentation of skeletal muscle CSA can be automated by utilizing a deep learning system.
- *Results:* The deep learning system automated the segmentation of skeletal muscle CSA and achieved an average DSC of 0.93 ($SD \pm 0.02$) and CSA error of 3.68 % ($SD \pm 2.29$).
- *Conclusion:* The fine-tuned deep learning system was able to mimic segmentation quality of experts for every new image.

Figure 11. High-level overview of the studies conducted as part of this thesis including the results. CSA = cross-sectional area; CT = computed tomography; DSC = Dice similarity coefficient; FACT-G = Functional Assessment of Cancer Therapy - General; HADS = Hospital Anxiety and Depression Scale; IMAT = intermuscular adipose tissue; IV = intravenous; L3SMI = skeletal muscle index at

the level of the third lumbar vertebral body; LOS = length of stay; SAT = subcutaneous adipose tissue; *SD* = standard deviation; SMD = skeletal muscle density; VAT = visceral adipose tissue.

4.2 Lean muscle mass and clinical outcomes

The findings in study A highlight the importance of lean muscle mass for respiratory outcomes. Study A showed that low skeletal muscle mass is associated with higher rates of pneumonia (16) which adds to the prior literature linking muscle weakness and symptomatic aspiration, typically presenting as pneumonitis or pneumonia (32). Our study relied on L3SMI, which is more objective than the clinical bedside assessments utilized in prior studies because L3SMI can be reliably measured on imaging, and there is no need for patient cooperation. Thus, there is less room for influencing biases. In addition, patients who were reintubated within 72 h post-extubation had significantly lower L3SMI. It has previously been assumed that decreased muscle mass has a negative impact on physiological ventilation (15). This study was the first to show a connection between low lean muscle mass and higher reintubation rates as well as pneumonia. Effective management of muscle weakness may have the potential to become a new target for the prevention of aspiration pneumonia and subsequent respiratory complications. To date, little is known about the importance of sarcopenia for respiratory muscles. A more comprehensive understanding of the underlying mechanisms may lead to treatment strategies that focus on preserving well-functioning muscles, such as early integration of physical therapy or dietary and nutrition services.

Study A was the first to establish that lower L3SMI is independently associated with increased total hospital costs (16). Previous studies described the association between increased hospital costs and decreased muscle area (4, 27). In the ICU setting, study A was the first to establish a link between low L3SMI and increased total hospital costs. Study A was also the first to demonstrate that low L3SMI is a predictor of increased hospital LOS post-extubation. This finding further supports the association between low muscle mass and increased utilization of health care resources. Appropriate allocation of health care resources is of growing importance as the costs of health care services increase (33). Body composition analysis, including muscle indices derived from CT, has the potential to improve clinical risk prediction and inform physicians which patients are at high risk of sarcopenia-related complications. Therefore, indices like L3SMI may help to inform the allocation of health care resources.

A previous study reported the association between skeletal muscle index and discharge disposition in trauma patients over 80 years (34). Compared to the univariable analysis used in the previous study, study A provides evidence that L3SMI is a predictor of adverse discharge disposition by using a multivariable model and controlling for comorbidities (16). What is more, our study includes younger patients (mean of 56.3 years, *SD* ± 18.9) from a wider variety of diagnostic categories (non-surgical

and elective surgery in addition to emergency trauma surgery included in the previous study [34]). Our findings suggest that muscle mass can help to predict adverse discharge disposition in ICU patients from a wide age range and various diagnostic categories. In an exploratory analysis, we utilized only age as a covariate, given that CCI and APACHE II score are often not available at the bedside. This simplified model did maintain its predictive power and might become clinically useful once the integration of deep-learning-based segmentation algorithms makes muscle measurements readily available in clinical practice (24).

To the best of our knowledge, study B first reported the association between sarcopenia, objectively measured on routine CT scans, and worse quality of life as well as increased depression symptoms in patients with advanced cancer. Sarcopenia and the associated physical decline have been previously proposed to negatively impact patients' QoL (35). Our study provides evidence to support this hypothesis by establishing an association between objective measurements of sarcopenia and patients' QoL. In addition, patients' increased physical activity has previously been linked to decreased depression symptoms (36). These findings may provide a mechanism explaining the association between sarcopenia and worse depression symptoms in our patient population. The majority of patients with advanced cancer (55.3 %) fulfilled the criteria for sarcopenia (18). Our findings highlight the need to screen patients with newly diagnosed advanced cancer for sarcopenia to address their functional status early in the course of their treatment. By screening for sarcopenia, potentially by using CT scans that are already part of routine care, patients at risk for low functional status and poor emotional well-being can be identified, and their care plans can be tailored to their needs. Therefore, addressing the highly prevalent issue of sarcopenia in patients with advanced disease early on can enable physicians to support these patients better and improve their quality of care.

4.3 Influencing factors of body composition analysis

Studies C and D systematically present the effect of modifiable CT acquisition parameters on threshold-based segmentation of muscle and adipose tissue, respectively. It may seem intuitive that CT acquisition parameters, such as IV contrast, slice thickness, tube current, and tube potential affect the computation of body composition indices. However, these effects have not been evaluated sufficiently. By comparing CSA and mean attenuation of skeletal muscle in study C and three adipose tissue compartments in study D, we add to the literature and provide a comprehensive evaluation of the effects of CT acquisition parameters on body composition indices. It is important to establish that the influence of CT acquisition parameters on these indices is significant. Previous studies established that body composition indices computed from CT images are associated with relevant clinical

outcomes in surgery (4), oncology (6), and ICU patients (2) but none of the referenced studies specified the CT protocols and acquisition parameters used to acquire the underlying CT scans.

Study C showed that muscle CSA is decreased by 4.8 %, and SMD is increased by 46.5 % on low-dose images compared to diagnostic CT images (19). This difference in low-dose images likely occurs due to a reduced signal-to-noise ratio. This high noise in the low-dose technique leads to a change in the distribution of pixels between HU values and affects the output of subsequent threshold-based segmentation of these images (as presented in figure 8A). SMD on 5 mm diagnostic CT slices is decreased by 11.6 %, and CSA is increased by 1.1 % compared to 2 mm slices (19). Partial volume averaging is less prominent on thinner slices. Therefore, thinner slices are expected to provide a more accurate measurement. However, an increased spread of the pixel distribution between HU values can be observed on 2 mm slices compared to 5 mm slices (figure 8B). Additionally, SMD is increased by 6.0 % and CSA by 1.9 % when IV contrast is present (19). This difference is likely due to the increased HU values of muscle fibers when a high-density contrast medium is present in the circulation. Muscle compartments below the HU threshold on non-contrast images then meet the threshold on contrast-enhanced images, which is represented by a rightward shift of the pixel distribution between HU values (figure 8C).

The findings in study D show that an increased slice thickness affects the mean attenuation of all adipose tissue compartments (21). To the best of our knowledge, study D was also the first to show that tube potential significantly affects both, adipose tissue CSA and mean attenuation measurement in all three adipose tissue compartments. In addition, it evaluates the effect of IV contrast on SAT and IMAT measurements. It is essential to distinguish between the body composition measures of adipose tissue compartments. CSA for VAT and SAT are considered adiposity measures and correlate with adiponectin and leptin levels (37). High IMAT CSA is an indicator of poor muscle quality. The mean attenuation values for adipose tissue compartments are indicators of the metabolic state. For example, a higher mean attenuation of VAT and SAT compartments is associated with smaller adipocytes and lower serum leptin levels (22).

Neglecting the influence of CT acquisition parameters on threshold-based segmentation can introduce systemic errors when comparing CT images that were acquired with different parameters. For example, study C quantified the mean difference in SMD between 2 mm and 5 mm CT slices as 2.36 HU (19). A recent study utilizing IV contrast-enhanced CTs of patients suffering from non-small-cell lung cancer postulated that a 1 HU increase in SMD was associated with a 2 % lower mortality rate (38). However, the slice thickness of the CT examinations is not specified in the respective study. According to this study (38), if images were acquired with different protocols regarding slice thickness (2 mm

and 5 mm), then about 4 % of the observed difference in mortality rate could solely be attributed to the difference in slice thickness. This shows the importance of potential systemic errors in studies that use threshold-based segmentation with inconsistent CT acquisition protocols. Furthermore, longitudinal analyses of the same patient can also be distorted if varying CT acquisition protocols are used over time. Unless identical protocols are used, serial measurements could fail to detect slight differences between images. CT acquisition protocols should be reported, and the effect of varying CT acquisition parameters should be scrutinized when body composition indices are used in research or clinical practice.

4.4 Fully automated segmentation system for skeletal muscle

Accurate segmentation of skeletal muscle in a semi-automated threshold-based fashion requires about 20 minutes per CT image on average (24). Our previous studies (A-D) rely on the manual labor of domain experts, which places a financial and time-intensive burden on transferring this measurement into clinical practice. In order to overcome this limitation, a rapid muscle segmentation pipeline is needed, which requires minor to no user interaction. The most recently proposed algorithms for the segmentation of muscles at the L3 level require less than one minute to process an abdominal region study (39). Our system requires only 0.17 seconds per CT image on average and enables near-instantaneous segmentation of skeletal muscle. The integration of body composition analysis into clinical practice has so far been limited by the resources needed to acquire the data. Body composition analysis of skeletal muscle is associated with a wide variety of important clinical outcomes (1-6, 40) and emerged as a valuable tool for risk stratification. CT is an essential technology in the current healthcare environment, and millions of CT examinations are performed each year. Utilizing this enormous data pool may improve the risk stratification of patients, which is essential for the advancement of personalized medicine. Enabling instantaneous muscle segmentation can help radiologists facilitate the transition of body composition analysis from research applications into clinical practice.

4.5 Limitations

The five studies presented above have several limitations worth considering. First, not all ICU patients had CT examinations available within five days of extubation in study A, which may have resulted in the preferred inclusion of sicker patients. Second, ICD-9 diagnosis codes were used to establish the diagnosis of pneumonia, which may have overestimated the true incidence of this primary outcome (16). Third, the study population of study B comprised patients solely from the Harvard Cancer Center, a large but single academic cancer center with limited racial and ethnic diversity. We cannot make assumptions about the generalizability of our findings to more heterogeneous populations. Fourth, in this randomized clinical trial, patients that already received palliative services or needed immediate hospice referral were excluded. These patients may have had more severe disease, which may have led to the underestimation of sarcopenia prevalence within palliative care patients in study B. Fifth, because of its cross-sectional nature, Study B can only report associations between patients' QoL and mood (18). It cannot provide information about the directionality of the relationships.

The first limitation for studies C and D is that the sample sizes, including 216 and 244 images, respectively, are relatively small. However, at the MGH, they are the largest sample of consecutive examinations, which was acquired using identical imaging protocols. Second, we did not evaluate the influence of IV contrast dose in both studies since bolus volume and contrast phase were kept constant. Third, images were acquired using automatic exposure control, which is common for routine imaging (19, 21). Therefore, the difference between contrast-enhanced and non-contrast CT examinations likely includes a variation in tube current.

The fully automated deep learning system proposed in Study E exhibits great potential for accelerating the computation of body composition indices, but there are limitations. First, the system tends to underestimate muscle CSA, which can probably be explained by overlapping HU values of muscle and neighboring organs and the variable appearance of organs. Especially in critically ill and obese patients with extensive soft-tissue edema, the system tends to overestimate muscle CSA due to the radiographic appearance of edema, which exhibits HU values within the HU thresholds for muscle. Second, the fully automated deep learning system was trained on data of a lung cancer cohort because the clinical protocol required these patients to undergo an abdominal CT scan with similar CT acquisition parameters. Third, the average age within this cohort was 63 years ($SD \pm 12$) which is expected for a lung cancer cohort (24). Further studies are warranted to assess whether the segmentation system can be generalized for different age groups.

4.6 Future directions

Building on the knowledge that lean muscle mass is a predictor of important surgical outcomes, the Fintelmann Lab at the MGH, where the presented five studies were conducted, strives to implement body composition indices into risk stratification models for surgical interventions. The goal is to improve personalized risk assessments for patients in order to provide them with the resources they need. The team is further working on automated segmentation systems for body composition analyses and has created an advanced software tool as well as the MGH-file format in the process. The Fintelmann Lab aims to aid the transition of body composition analysis from research applications into clinical practice.

The research questions investigated as part of this MD/PhD thesis yield the potential for exciting future research. Ethnic diversity was limited in the study population of study B. Further studies are needed to evaluate the issue of sarcopenia among a more heterogeneous population of patients with cancer. Additionally, study B does not support statements about the directionality of the relationship between sarcopenia and patients' QoL because of its cross-sectional design (18). A longitudinal study, which evaluates how changes in muscle mass throughout the cancer treatment affect patients' QoL and mood, could provide a deeper insight into the importance of sarcopenia. It could be essential to understand in which ways sarcopenia affects patient outcomes and what additional interventions are needed to improve the supportive care of patients with advanced cancer.

Another crucial topic is the implementation of best practices for imaging protocols used in body composition analysis. Based on study C, diagnostic quality IV-contrast enhanced CT scans are presumably most suitable for the analysis of skeletal muscle (19). Further studies are required to establish the ideal CT acquisition parameters for body composition analysis. The standardization of imaging protocols will facilitate the comparability between clinical trials and enable researchers to determine generalizable reference values. For example, the currently proposed L3SMI cut-off values for sarcopenia (31) might only apply for specific imaging protocols. The standardization of imaging protocols will help to interpret results from body composition analysis correctly and to prevent systematic errors.

Furthermore, the automation of adipose tissue segmentation is an exciting new target. The HU threshold range for adipose tissue (-190 to -30 HU [13]) is considerably specific and enables the algorithms to segment fat reliably. In order to accurately differentiate between SAT and VAT compartments, precise determination of muscular boundaries is required, which can be generated by the segmentation of skeletal muscle. The combination of an adipose tissue thresholding system with our fully automated muscle segmentation system could accurately provide data on adipose tissue compartments in addition to information on skeletal muscle. Our segmentation system could also be enhanced to a whole-body

volumetric analysis in order to provide a comprehensive analysis of a patient's body composition. With versatile, automatic segmentation tools, as proposed in study E (24), there is the potential to integrate body composition analysis into clinical practice.

5 Conclusion

In summary, the lumbar skeletal muscle index is a useful tool for the assessment of muscle mass in clinical practice and can be reliably computed from routine abdominal CT scans. In critically ill patients, lower L3SMI was associated with worse clinical outcomes and can add clinically useful information at the time of extubation. For patients with advanced cancer, L3SMI can aid the clinical diagnosis of sarcopenia, which affected most patients in our oncologic study population. Patients with advanced cancer who suffered from sarcopenia reported increased depression symptoms and worse quality of life. This highlights the clinical relevance of addressing muscle loss early on as part of a multimodal treatment plan. Importantly, L3SMI and other indices utilized in body composition analysis are significantly affected by CT acquisition parameters. Intravenous contrast, slice thickness, tube current, and tube potential influence the quantification and characterization of muscle mass and adipose tissue. These effects of CT acquisition parameters should be considered when body composition analysis is used in clinical practice or research studies. Finally, our fully automated deep learning system achieved excellent agreement with images segmented by domain experts and enabled instantaneous segmentation of skeletal muscle.

6 References

1. Weijs PJ, Looijaard WG, Dekker IM, Stapel SN, Girbes AR, Oudemans-van Straaten HM, Beishuizen A. Low skeletal muscle area is a risk factor for mortality in mechanically ventilated critically ill patients. *Critical Care.* 2014;18(2):R12.

2. Moisey LL, Mourtzakis M, Cotton BA, Premji T, Heyland DK, Wade CE, Bulger E, Kozar RA. Skeletal muscle predicts ventilator-free days, ICU-free days, and mortality in elderly ICU patients. *Critical Care.* 2013;17(5):R206.

3. Reisinger KW, Bosmans JW, Uittenbogaart M, Alsoumali A, Poeze M, Sosef MN, Derikx JP. Loss of Skeletal Muscle Mass During Neoadjuvant Chemoradiotherapy Predicts Postoperative Mortality in Esophageal Cancer Surgery. *Annals of Surgical Oncology.* 2015;22(13):4445-4452.

4. Englesbe MJ, Lee JS, He K, Fan L, Schaubel DE, Sheetz KH, Harbaugh CM, Holcombe SA, Campbell DA, Jr., Sonnenday CJ, Wang SC. Analytic Morphomics, Core Muscle Size, and Surgical Outcomes. *Annals of Surgery.* 2012;256(2):255-261.

5. Martin L, Birdsell L, Macdonald N, Reiman T, Clandinin MT, McCargar LJ, Murphy R, Ghosh S, Sawyer MB, Baracos VE. Cancer Cachexia in the Age of Obesity: Skeletal Muscle Depletion Is a Powerful Prognostic Factor, Independent of Body Mass Index. *Journal of Clinical Oncology.* 2013;31(12):1539-1547.

6. Prado CM, Lieffers JR, McCargar LJ, Reiman T, Sawyer MB, Martin L, Baracos VE. Prevalence and clinical implications of sarcopenic obesity in patients with solid tumours of the respiratory and gastrointestinal tracts: a population-based study. *Lancet Oncology.* 2008;9(7):629-635.

7. Farhan H, Moreno-Duarte I, Latronico N, Zafonte R, Eikermann M. Acquired Muscle Weakness in the Surgical Intensive Care Unit: Nosology, Epidemiology, Diagnosis, and Prevention. *Anesthesiology.* 2016;124(1):207-234.

8. Connolly BA, Jones GD, Curtis AA, Murphy PB, Douiri A, Hopkinson NS, Polkey MI, Moxham J, Hart N. Clinical predictive value of manual muscle strength testing during critical illness: an observational cohort study. *Critical Care.* 2013;17(5):R229.

9. Prado CM, Heymsfield SB. Lean Tissue Imaging: A New Era for Nutritional Assessment and Intervention. *Journal of Parenteral and Enteral Nutrition.* 2014;38(8):940-953.

10. Cruz-Jentoft AJ, Sayer AA. Sarcopenia. *Lancet.* 2019;393(10191):2636-2646.

11. Cruz-Jentoft AJ, Bahat G, Bauer J, Boirie Y, Bruyere O, Cederholm T, Cooper C, Landi F, Rolland Y, Sayer AA, Schneider SM, Sieber CC, Topinkova E, Vandewoude M, Visser M, Zamboni M. Sarcopenia: revised European consensus on definition and diagnosis. *Age and Ageing.* 2019;48(1):16-31.

12. Mourtzakis M, Prado CM, Lieffers JR, Reiman T, McCargar LJ, Baracos VE. A practical and precise approach to quantification of body composition in cancer patients using computed tomography images acquired during routine care. *Applied Physiology, Nutrition, and Metabolism.* 2008;33(5):997-1006.

13. Mitsiopoulos N, Baumgartner RN, Heymsfield SB, Lyons W, Gallagher D, Ross R. Cadaver validation of skeletal muscle measurement by magnetic resonance imaging and computerized tomography. *Journal of Applied Physiology.* 1998;85(1):115-122.

14. Shen W, Punyanitya M, Wang Z, Gallagher D, St-Onge MP, Albu J, Heymsfield SB, Heshka S. Total body skeletal muscle and adipose tissue volumes: estimation from a single abdominal cross-sectional image. *Journal of Applied Physiology.* 2004;97(6):2333-2338.

15. Enright S, Chatham K, Ionescu AA, Unnithan VB, Shale DJ. The influence of body composition on respiratory muscle, lung function and diaphragm thickness in adults with cystic fibrosis. *Journal of Cystic Fibrosis.* 2007;6(6):384-390.

16. Fuchs G, Thevathasan T, Chretien YR, Mario J, Piriyapatsom A, Schmidt U, Eikermann M, Fintelmann FJ. Lumbar skeletal muscle index derived from routine computed tomography exams predict adverse post-extubation outcomes in critically ill patients. *Journal of Critical Care.* 2018;44:117-123.

17. Janssen I, Heymsfield SB, Ross R. Low Relative Skeletal Muscle Mass (Sarcopenia) in Older Persons Is Associated with Functional Impairment and Physical Disability. *Journal of the American Geriatrics Society.* 2002;50(5):889-896.

18. Nipp RD, Fuchs G, El-Jawahri A, Mario J, Troschel FM, Greer JA, Gallagher ER, Jackson VA, Kambadakone A, Hong TS, Temel JS, Fintelmann FJ. Sarcopenia Is Associated with Quality of Life and Depression in Patients with Advanced Cancer. *Oncologist.* 2018;23(1):97-104.

19. Fuchs G, Chretien YR, Mario J, Do S, Eikermann M, Liu B, Yang K, Fintelmann FJ. Quantifying the effect of slice thickness, intravenous contrast and tube current on muscle segmentation: Implications for body composition analysis. *European Radiology.* 2018;28(6):2455-2463.

20. Antoun S, Lanoy E, Iacovelli R, Albiges-Sauvin L, Loriot Y, Merad-Taoufik M, Fizazi K, di Palma M, Baracos VE, Escudier B. Skeletal Muscle Density Predicts Prognosis in Patients With Metastatic Renal Cell Carcinoma Treated With Targeted Therapies. *Cancer.* 2013;119(18):3377-3384.

21. Troschel AS, Troschel FM, Fuchs G, Marquardt JP, Ackman JB, Yang K, Fintelmann FJ. Significance of Acquisition Parameters for Adipose Tissue Segmentation on CT Images. *American Journal of Roentgenology.* 2021;217(1):177-185.

22. Murphy RA, Register TC, Shively CA, Carr JJ, Ge Y, Heilbrun ME, Cummings SR, Koster A, Nevitt MC, Satterfield S, Tylvasky FA, Strotmeyer ES, Newman AB, Simonsick EM, Scherzinger A, Goodpaster BH, Launer LJ, Eiriksdottir G, Sigurdsson S, Sigurdsson G, Gudnason V, Lang TF, Kritchevsky SB, Harris TB. Adipose Tissue Density, a Novel Biomarker Predicting Mortality Risk in Older Adults. *Journals of Gerontology Series A: Biological Sciences and Medical Sciences.* 2014;69(1):109-117.

23. Von Hessen L, Roumet M, Maurer MH, Lange N, Reeves H, Dufour JF, Radu P. High subcutaneous adipose tissue density correlates negatively with survival in patients with hepatocellular carcinoma. *Liver International.* 2021;41(4):828-836.

24. Lee H, Troschel FM, Tajmir S, Fuchs G, Mario J, Fintelmann FJ, Do S. Pixel-Level Deep Segmentation: Artificial Intelligence Quantifies Muscle on Computed Tomography for Body Morphometric Analysis. *Journal of Digital Imaging.* 2017;30(4):487-498.

25. Greenspan H, van Ginneken B, Summers RM. Guest Editorial Deep Learning in Medical Imaging: Overview and Future Promise of an Exciting New Technique. *IEEE Transactions on Medical Imaging.* 2016;35(5):1153-1159.

26. Temel JS, Greer JA, El-Jawahri A, Pirl WF, Park ER, Jackson VA, Back AL, Kamdar M, Jacobsen J, Chittenden EH, Rinaldi SP, Gallagher ER, Eusebio JR, Li Z, Muzikansky A, Ryan DP. Effects of Early Integrated Palliative Care in Patients With Lung and GI Cancer: A Randomized Clinical Trial. *Journal of Clinical Oncology.* 2017;35(8):834-841.

27. Mueller N, Murthy S, Tainter CR, Lee J, Riddell K, Fintelmann FJ, Grabitz SD, Timm FP, Levi B, Kurth T, Eikermann M. Can Sarcopenia Quantified by Ultrasound of the Rectus Femoris Muscle Predict Adverse Outcome of Surgical Intensive Care Unit Patients as well as Frailty? A Prospective, Observational Cohort Study. *Annals of Surgery.* 2016;264(6):1116-1124.

28. Cella DF, Tulsky DS, Gray G, Sarafian B, Linn E, Bonomi A, Silberman M, Yellen SB, Winicour P, Brannon J, Eckberg K, Lloyd S, Purl S, Blendowski C, Goodman M, Barnicle M, Stewart I, McHale M, Bonomi P, Kaplan E, Taylor S, Thomas CR, Harris J. The Functional Assessment of Cancer Therapy scale: Development and Validation of the General Measure. *Journal of Clinical Oncology.* 1993;11(3):570-579.

29. Zigmond AS, Snaith RP. The hospital anxiety and depression scale. *Acta Psychiatrica Scandinavica.* 1983;67(6):361-370.

30. Bland JM, Altman DG. Statistical methods for assessing agreement between two methods of clinical measurement. *Lancet.* 1986;1(8476):307-310.

31. Fearon K, Strasser F, Anker SD, Bosaeus I, Bruera E, Fainsinger RL, Jatoi A, Loprinzi C, MacDonald N, Mantovani G, Davis M, Muscaritoli M, Ottery F, Radbruch L, Ravasco P, Walsh D, Wilcock A, Kaasa S, Baracos VE. Definition and classification of cancer cachexia: an international consensus. *Lancet Oncology.* 2011;12(5):489-495.

32. Mirzakhani H, Williams JN, Mello J, Joseph S, Meyer MJ, Waak K, Schmidt U, Kelly E, Eikermann M. Muscle Weakness Predicts Pharyngeal Dysfunction and Symptomatic Aspiration in Long-term Ventilated Patients. *Anesthesiology.* 2013;119(2):389-397.

33. Anderson JL, Heidenreich PA, Barnett PG, Creager MA, Fonarow GC, Gibbons RJ, Halperin JL, Hlatky MA, Jacobs AK, Mark DB, Masoudi FA, Peterson ED, Shaw LJ. ACC/AHA Statement on Cost/Value Methodology in Clinical Practice Guidelines and Performance Measures: A Report of the American College of Cardiology/American Heart Association Task Force on Performance Measures and Task Force on Practice Guidelines. *Journal of the American College of Cardiology.* 2014;63(21):2304-2322.

34. Du Y, Karvellas CJ, Baracos V, Williams DC, Khadaroo RG. Sarcopenia is a predictor of outcomes in very elderly patients undergoing emergency surgery. *Surgery.* 2014;156(3):521-527.

35. Beaudart C, Reginster JY, Petermans J, Gillain S, Quabron A, Locquet M, Slomian J, Buckinx F, Bruyere O. Quality of life and physical components linked to sarcopenia: The SarcoPhAge study. *Experimental Gerontology.* 2015;69:103-110.

36. Brown JC, Huedo-Medina TB, Pescatello LS, Ryan SM, Pescatello SM, Moker E, LaCroix JM, Ferrer RA, Johnson BT. The Efficacy of Exercise in Reducing Depressive Symptoms among Cancer Survivors: A Meta-Analysis. *PloS One.* 2012;7(1):e30955.

37. Lee JJ, Britton KA, Pedley A, Massaro JM, Speliotes EK, Murabito JM, Hoffmann U, Ingram C, Keaney JF, Jr., Vasan RS, Fox CS. Adipose Tissue Depots and Their Cross-Sectional Associations With Circulating Biomarkers of Metabolic Regulation. *Journal of the American Heart Association.* 2016;5(5).

38. Sjoblom B, Gronberg BH, Wentzel-Larsen T, Baracos VE, Hjermstad MJ, Aass N, Bremnes RM, Flotten O, Bye A, Jordhoy M. Skeletal muscle radiodensity is prognostic for survival in patients with advanced non-small cell lung cancer. *Clinical Nutrition.* 2016;35(6):1386-1393.

39. Graffy PM, Liu J, Pickhardt PJ, Burns JE, Yao J, Summers RM. Deep learning-based muscle segmentation and quantification at abdominal CT: application to a longitudinal adult screening cohort for sarcopenia assessment. *British Journal of Radiology.* 2019;92(1100):20190327.

40. Fehrenbach U, Wuensch T, Gabriel P, Segger L, Yamaguchi T, Auer TA, Beetz NL, Denecke C, Kroll D, Raakow J, Knitter S, Chopra S, Thuss-Patience P, Pratschke J, Hamm B, Biebl M, Geisel D. CT Body Composition of Sarcopenia and Sarcopenic Obesity: Predictors of Postoperative Complications and Survival in Patients with Locally Advanced Esophageal Adenocarcinoma. *Cancers.* 2021;13(12).

Affidavit

„Ich, Georg Fuchs, versichere an Eides statt durch meine eigenhändige Unterschrift, dass ich die vorgelegte Dissertation mit dem Thema: „Body Composition Analysis: Skeletal Muscle Measurement with Computed Tomography and Implications for Patient Care / Analyse der Körperzusammensetzung: Messung der Skelettmuskulatur mit Computertomographie und Implikationen für die Patientenversorgung“ selbstständig und ohne nicht offengelegte Hilfe Dritter verfasst und keine anderen als die angegebenen Quellen und Hilfsmittel genutzt habe.

Alle Stellen, die wörtlich oder dem Sinne nach auf Publikationen oder Vorträgen anderer Autoren/innen beruhen, sind als solche in korrekter Zitierung kenntlich gemacht. Die Abschnitte zu Methodik (insbesondere praktische Arbeiten, Laborbestimmungen, statistische Aufarbeitung) und Resultaten (insbesondere Abbildungen, Graphiken und Tabellen) werden von mir verantwortet.

Ich versichere ferner, dass ich die in Zusammenarbeit mit anderen Personen generierten Daten, Datenauswertungen und Schlussfolgerungen korrekt gekennzeichnet und meinen eigenen Beitrag sowie die Beiträge anderer Personen korrekt kenntlich gemacht habe (siehe Anteilserklärung). Texte oder Textteile, die gemeinsam mit anderen erstellt oder verwendet wurden, habe ich korrekt kenntlich gemacht.

Meine Anteile an etwaigen Publikationen zu dieser Dissertation entsprechen denen, die in der untenstehenden gemeinsamen Erklärung mit dem/der Erstbetreuer/in, angegeben sind. Für sämtliche im Rahmen der Dissertation entstandenen Publikationen wurden die Richtlinien des ICMJE (International Committee of Medical Journal Editors; www.icmje.og) zur Autorenschaft eingehalten. Ich erkläre ferner, dass ich mich zur Einhaltung der Satzung der Charité – Universitätsmedizin Berlin zur Sicherung Guter Wissenschaftlicher Praxis verpflichte.

Weiterhin versichere ich, dass ich diese Dissertation weder in gleicher noch in ähnlicher Form bereits an einer anderen Fakultät eingereicht habe.

Die Bedeutung dieser eidesstattlichen Versicherung und die strafrechtlichen Folgen einer unwahren eidesstattlichen Versicherung (§§156, 161 des Strafgesetzbuches) sind mir bekannt und bewusst.“

Richterswil, den 22.08.2022 Georg Fuchs

Detailed declaration of contribution

Georg Fuchs hatte den folgenden Anteil an den fünf Publikationen:

Publikation A: Fuchs G, Thevathasan T, Chretien YR, Mario J, Piriyapatsom A, Schmidt U, Eikermann M, Fintelmann FJ. **Lumbar Skeletal Muscle Index Derived from Routine Computed Tomography Exams Predict Adverse Post-Extubation Outcomes in Critically Ill Patients.** *Journal of Critical Care.* 2018;44:117-123.

Beitrag im Einzelnen: Software-basierte Analyse aller CT-Bilder mit OsiriX und Segmentierung der Muskelmasse; Erarbeitung aller in der Publikation verwendeten Abbildungen (1-6) und Tabellen (1-5); Erarbeitung der gesamten Erstfassung des Manuskripts inklusive der Literaturauswahl; Revision des Manuskripts mithilfe der Anmerkungen der Ko-Autoren; Entwicklung der Fragestellung mit Unterstützung von Prof. Fintelmann; Literaturrecherche; Konzept und Design der Studie sowie des Studienprotokolls mit Unterstützung von Prof. Fintelmann und in Diskussionen mit dem Studienteam; Erarbeitung und Einreichung des Ethikantrags mit Unterstützung von Prof. Fintelmann; Projektmanagement des Studienteams; Charakterisierung der Studienkohorte, Definition der Einschluss- und Ausschlusskriterien; Definition der statistischen Auswertung; Sammlung der Daten mit Unterstützung von T. Thevathasan; Aufarbeitung der Daten; Durchsicht und Interpretation der klinischen Bildgebung mit Unterstützung von Prof. Fintelmann; Analyse aller CT-Bilder für die Intrarater-Reliabilitätsanalyse; statistische Auswertung der Daten mit Unterstützung von T. Thevathasan; Diskussion der Ergebnisse mit Dr. Chretien (Statistiker der Arbeitsgruppe und Radiologe); kritische Interpretation der Ergebnisse mit Unterstützung von Prof. Fintelmann und Vorbereitung der Diskussionen im Studienteam; Design und Durchführung der Datenvisualisierung; Einreichung des Manuskripts bei der Zeitschrift Journal of Critical Care; Revision des Manuskripts mit Unterstützung von Prof. Fintelmann und Adressierung der Reviewer-Kommentare.

Publikation B: Nipp RD, Fuchs G, El-Jawahri A, Mario J, Troschel FM, Greer JA, Gallagher ER, Jackson VA, Kambadakone A, Hong TS, Temel JS, Fintelmann FJ. **Sarcopenia Is Associated with Quality of Life and Depression in Patients with Advanced Cancer.** *Oncologist.* 2018;23(1):97-104.

Beitrag im Einzelnen: Software-basierte Analyse aller CT-Bilder mit OsiriX und Segmentierung der Muskelmasse; Erarbeitung der in der Publikation verwendeten Abbildungen 1A und B; alle Tabellen (1-3) basieren auf den Ergebnissen meiner radiologischen Analysen in Kombination mit Daten der Studiendatenbank; Abbildung 2 basiert auf den Ergebnissen meiner radiologischen Analysen in Kombination mit Daten der Studiendatenbank; die Erstfassung des Manuskripts erstellte ich gemeinsam mit

Dr. Nipp; alle Textpassagen zur radiologischen Bildgebung und deren Analyse wurden ausschließlich von mir erstellt; Sammlung der Daten gemeinsam mit Dr. Nipp; Aufarbeitung der Daten gemeinsam mit Dr. Nipp; statistische Auswertung der Daten gemeinsam mit Dr. Nipp; Revision des Manuskripts mithilfe der Anmerkungen der Ko-Autoren gemeinsam mit Dr. Nipp; Entwicklung der Fragestellung gemeinsam mit Prof. Fintelmann und Dr. Nipp; Literaturrecherche gemeinsam mit Dr. Nipp; Konzept und Design der Studie und des Studienprotokolls gemeinsam mit Prof. Fintelmann und Dr. Nipp; Projektmanagement des Studienteams gemeinsam mit Dr. Nipp; Charakterisierung der Studienkohorte sowie Definition der Einschluss- und Ausschlusskriterien gemeinsam mit Dr. Nipp; Definition der statistischen Auswertung gemeinsam mit Dr. Nipp; Durchsicht und Interpretation der klinischen Bildgebung mit Unterstützung von Prof. Fintelmann; Analyse der CT-Bilder für die Intrarater-Reliabilitätsanalyse; Kritische Interpretation der Ergebnisse gemeinsam mit Dr. Nipp und Prof. Fintelmann; Vorbereitung der Diskussionen im Studienteam; Design und Durchführung der Datenvisualisierung gemeinsam mit Dr. Nipp; Revision des Manuskripts und Adressierung der Reviewer-Kommentare gemeinsam mit Dr. Nipp.

Publikation C: Fuchs G, Chretien YR, Mario J, Do S, Eikermann M, Liu B, Yang K, Fintelmann FJ. **Quantifying the Effect of Slice Thickness, Intravenous Contrast and Tube Current on Muscle Segmentation: Implications for Body Composition Analysis.** *European Radiology*. 2018;28(6):2455-2463.

Beitrag im Einzelnen: Software-basierte Analyse aller CT-Bilder mit OsiriX und Segmentierung der Muskelmasse; Sammlung aller Daten; Aufarbeitung aller Daten; gesamte statistische Auswertung der Daten; Erarbeitung aller in der Publikation verwendeten Abbildungen (1-6); Erarbeitung der gesamten Erstfassung des Manuskripts inklusive der Literaturauswahl; Revision des Manuskripts mithilfe der Anmerkungen der Ko-Autoren; Entwicklung der Fragestellung mit Unterstützung von Prof. Fintelmann; Literaturrecherche; Konzept und Design der Studie und des Studienprotokolls mit Unterstützung von Prof. Fintelmann; Erarbeitung und Einreichung des Ethikantrags; Projektmanagement des Studienteams; Charakterisierung der Studienkohorte sowie Definition der Einschluss- und Ausschlusskriterien; Definition der statistischen Auswertung; Durchsicht und Interpretation der klinischen Bildgebung mit Unterstützung von Prof. Fintelmann; Analyse der CT-Bilder für die Intrarater-Reliabilitätsanalyse; Diskussion der Ergebnisse mit Yves Chretien (Statistiker der Arbeitsgruppe und Radiologe); kritische Interpretation der Ergebnisse mit Unterstützung von Prof. Fintelmann und Vorbereitung der Diskussionen im Studienteam; Design und Durchführung der Datenvisualisierung; Einreichung des Manuskripts bei der Zeitschrift European Radiology; Revision des Manuskripts und Adressierung der Reviewer-Kommentare.

Publikation D: Troschel AS, Troschel FM, Fuchs G, Marquardt JP, Ackman JB, Yang K, Fintelmann FJ. **Significance of Acquisition Parameters for Adipose Tissue Segmentation on CT Images.** *American Journal of Roentgenology.* 2021;217(1):177-185.

Beitrag im Einzelnen: Entwicklung der Fragestellung gemeinsam mit Amelie Troschel und Prof. Fintelmann; Konzept und Design der Studie und des Studienprotokolls gemeinsam mit Amelie Troschel und Prof. Fintelmann; Definition der statistischen Auswertung gemeinsam mit Amelie Troschel; Unterstützung bei der Sammlung der Daten; Unterstützung bei der statistischen Auswertung der Daten; Unterstützung bei der Interpretation der Ergebnisse; Unterstützung beim Design der Datenvisualisierung; Unterstützung bei der Erarbeitung der Erstfassung des Manuskripts; Unterstützung bei der Revision des Manuskripts; Unterstützung bei der Einreichung des Manuskripts; Unterstützung bei der Adressierung der Reviewer-Kommentare.

Publikation E: Lee H, Troschel FM, Tajmir S, Fuchs G, Mario J, Fintelmann FJ, Do S. **Pixel-Level Deep Segmentation: Artificial Intelligence Quantifies Muscle on Computed Tomography for Body Morphometric Analysis**. *Journal of Digital Imaging.* 2017;30(4):487-498.

Beitrag im Einzelnen: Entwicklung der Fragestellung gemeinsam mit Fabian Troschel und Prof. Fintelmann; Konzept und Design der Studie gemeinsam mit Fabian Troschel und Prof. Fintelmann; Unterstützung bei der Charakterisierung der Studienkohorte sowie bei der Sammlung der Daten; software-basierte Analyse von CT-Bildern mit OsiriX, Segmentierung der Muskelmasse und Bereitstellung von segmentierten CT-Bildern als Referenzstandard für das Training des Algorithmus; Unterstützung bei der Revision des Manuskripts.

Richterswil, den 22.08.2022 Georg Fuchs

Publications

Journal Data Filtered By: **Selected JCR Year: 2016** Selected Editions: SCIE,SSCI
Selected Categories: **"CRITICAL CARE MEDICINE"** Selected Category Scheme: WoS

Gesamtanzahl: 33 Journale

Rank	Full Journal Title	Total Cites	Journal Impact Factor	Eigenfactor Score
1	Lancet Respiratory Medicine	3,920	19.287	0.020520
2	AMERICAN JOURNAL OF RESPIRATORY AND CRITICAL CARE MEDICINE	56,793	13.204	0.090280
3	INTENSIVE CARE MEDICINE	20,100	12.015	0.035410
4	CRITICAL CARE MEDICINE	38,568	7.050	0.062590
5	CHEST	49,091	6.044	0.062880
6	CRITICAL CARE	19,632	5.358	0.048590
7	RESUSCITATION	12,023	5.230	0.023150
8	JOURNAL OF NEUROTRAUMA	12,787	5.190	0.021640
9	Annals of Intensive Care	1,158	3.656	0.005150
10	Pediatric Critical Care Medicine	4,991	3.495	0.010330
11	Journal of Trauma and Acute Care Surgery	6,228	3.403	0.026510
12	Current Opinion in Critical Care	3,063	3.316	0.006460
13	SHOCK	6,828	3.113	0.010480
14	Neurocritical Care	3,471	2.752	0.009480
15	JOURNAL OF CRITICAL CARE	4,694	2.648	0.013880
16	Minerva Anestesiologica	2,594	2.623	0.005430
17	SEMINARS IN RESPIRATORY AND CRITICAL CARE MEDICINE	1,836	2.614	0.004500
18	Critical Care and Resuscitation	833	2.520	0.002860
19	Human Gene Therapy Clinical Development	202	2.490	0.001000
20	ANASTHESIOLOGIE & INTENSIVMEDIZIN	472	2.227	0.000890
21	JOURNAL OF INTENSIVE CARE MEDICINE	1,150	2.156	0.002350
22	BURNS	7,044	2.056	0.007950
23	CRITICAL CARE CLINICS	1,559	1.927	0.002480
24	Australian Critical Care	520	1.907	0.000930

Publication A: Lumbar Skeletal Muscle Index Derived from Routine Computed Tomography Exams Predict Adverse Post-Extubation Outcomes in Critically Ill Patients

Fuchs G, Thevathasan T, Chretien YR, Mario J, Piriyapatsom A, Schmidt U, Eikermann M, Fintelmann FJ. *Journal of Critical Care.* 2018;44:117-123.

https://doi.org/10.1016/j.jcrc.2017.10.033

Journal Data Filtered By: **Selected JCR Year: 2016** Selected Editions: SCIE,SSCI
Selected Categories: **"ONCOLOGY"** Selected Category Scheme: WoS
Gesamtanzahl: 217 Journale

Rank	Full Journal Title	Total Cites	Journal Impact Factor	Eigenfactor Score
1	CA-A CANCER JOURNAL FOR CLINICIANS	24,539	187.040	0.064590
2	NATURE REVIEWS CANCER	46,017	37.147	0.084950
3	LANCET ONCOLOGY	38,110	33.900	0.121930
4	CANCER CELL	32,653	27.407	0.102930
5	JOURNAL OF CLINICAL ONCOLOGY	149,617	24.008	0.284800
6	Nature Reviews Clinical Oncology	6,733	20.693	0.026770
7	Cancer Discovery	8,944	20.011	0.053450
8	JAMA Oncology	2,496	16.559	0.011300
9	JNCI-Journal of the National Cancer Institute	38,391	12.589	0.062530
10	ANNALS OF ONCOLOGY	34,424	11.855	0.090980
11	LEUKEMIA	23,538	11.702	0.059800
12	CLINICAL CANCER RESEARCH	77,834	9.619	0.140990
13	BIOCHIMICA ET BIOPHYSICA ACTA-REVIEWS ON CANCER	4,889	9.452	0.009460
14	SEMINARS IN CANCER BIOLOGY	5,835	9.141	0.012370
15	CANCER RESEARCH	139,655	9.122	0.149180
16	CANCER TREATMENT REVIEWS	7,122	8.589	0.014420
17	Cancer Immunology Research	2,936	8.284	0.013910
18	Liver Cancer	565	7.854	0.001550
19	NEURO-ONCOLOGY	8,326	7.786	0.024280
20	OncoImmunology	4,157	7.719	0.015390
21	ONCOGENE	65,039	7.519	0.080060
22	JOURNAL OF PATHOLOGY	16,079	6.894	0.026950
23	Journal of Thoracic Oncology	12,094	6.595	0.032240
24	INTERNATIONAL JOURNAL OF CANCER	49,805	6.513	0.073930
25	CANCER LETTERS	26,657	6.375	0.040280
26	Journal of Hematology & Oncology	2,879	6.350	0.007920
27	BREAST CANCER RESEARCH	10,541	6.345	0.023850
28	Therapeutic Advances in Medical Oncology	787	6.294	0.002420
29	Advances in Cancer Research	2,187	6.267	0.003210
30	SEMINARS IN ONCOLOGY	5,448	6.212	0.008120
31	Molecular Cancer	9,134	6.204	0.018240
32	BRITISH JOURNAL OF CANCER	45,262	6.176	0.073220
33	Blood Cancer Journal	1,270	6.126	0.006320

Rank	Full Journal Title	Total Cites	Journal Impact Factor	Eigenfactor Score
34	EUROPEAN JOURNAL OF CANCER	27,303	6.029	0.048010
35	CANCER	66,326	5.997	0.074110
36	MOLECULAR CANCER THERAPEUTICS	18,257	5.764	0.033610
37	STEM CELLS	20,822	5.599	0.038100
38	Gastric Cancer	3,900	5.454	0.008430
39	SEMINARS IN RADIATION ONCOLOGY	2,232	5.356	0.003910
40	Molecular Oncology	3,895	5.314	0.012400
41	ENDOCRINE-RELATED CANCER	6,547	5.267	0.011550
42	JOURNAL OF EXPERIMENTAL & CLINICAL CANCER RESEARCH	4,593	5.189	0.006840
43	Pigment Cell & Melanoma Research	3,903	5.170	0.007990
44	Oncotarget	30,241	5.168	0.078720
45	INTERNATIONAL JOURNAL OF RADIATION ONCOLOGY BIOLOGY PHYSICS	44,068	5.133	0.060060
46	CARCINOGENESIS	21,584	5.105	0.026120
47	NEOPLASIA	6,701	5.006	0.010610
48	Clinical Epigenetics	1,322	4.987	0.004490
49	MOLECULAR CANCER RESEARCH	7,764	4.974	0.016460
50	CRITICAL REVIEWS IN ONCOLOGY HEMATOLOGY	6,296	4.971	0.011240
51	ONCOLOGIST	10,533	4.962	0.022230
52	GYNECOLOGIC ONCOLOGY	22,924	4.959	0.038520
53	ORAL ONCOLOGY	8,242	4.794	0.014210
54	CANCER IMMUNOLOGY IMMUNOTHERAPY	7,180	4.711	0.013690
55	CANCER AND METASTASIS REVIEWS	5,685	4.697	0.007270
56	Journal of the National Comprehensive Cancer Network	4,197	4.675	0.014320
57	Clinical Colorectal Cancer	1,046	4.507	0.002240
58	RADIOTHERAPY AND ONCOLOGY	15,639	4.328	0.028040
59	LUNG CANCER	10,841	4.294	0.019900
60	CANCER JOURNAL	2,824	4.218	0.006360
61	MOLECULAR CARCINOGENESIS	4,856	4.185	0.008000
62	Oncogenesis	877	4.143	0.003330
63	CANCER EPIDEMIOLOGY BIOMARKERS & PREVENTION	19,570	4.142	0.033440
64	Chinese Journal of Cancer	1,737	4.111	0.003910

Publication B: Sarcopenia Is Associated with Quality of Life and Depression in Patients with Advanced Cancer

Nipp RD, Fuchs G, El-Jawahri A, Mario J, Troschel FM, Greer JA, Gallagher ER, Jackson VA, Kambadakone A, Hong TS, Temel JS, Fintelmann FJ. *Oncologist.* 2018;23(1):97-104.

https://doi.org/10.1634/theoncologist.2017-0255

Journal Data Filtered By: **Selected JCR Year: 2016** Selected Editions: SCIE,SSCI Selected Categories: **"RADIOLOGY, NUCLEAR MEDICINE and MEDICAL IMAGING"** Selected Category Scheme: WoS

Gesamtanzahl: 126 Journale

Rank	Full Journal Title	Total Cites	Journal Impact Factor	Eigenfactor Score
1	JACC-Cardiovascular Imaging	6,895	10.189	0.027050
2	RADIOLOGY	50,983	7.296	0.066140
3	EUROPEAN JOURNAL OF NUCLEAR MEDICINE AND MOLECULAR IMAGING	14,019	7.277	0.024910
4	Circulation-Cardiovascular Imaging	4,472	6.803	0.019120
5	JOURNAL OF NUCLEAR MEDICINE	24,977	6.646	0.037540
6	NEUROIMAGE	85,630	5.835	0.173210
7	JOURNAL OF CARDIOVASCULAR MAGNETIC RESONANCE	4,349	5.601	0.014950
8	SEMINARS IN RADIATION ONCOLOGY	2,232	5.356	0.003910
9	INVESTIGATIVE RADIOLOGY	5,925	5.195	0.011230
10	INTERNATIONAL JOURNAL OF RADIATION ONCOLOGY BIOLOGY PHYSICS	44,068	5.133	0.060060
11	ULTRASOUND IN OBSTETRICS & GYNECOLOGY	11,611	4.710	0.019350
12	HUMAN BRAIN MAPPING	18,139	4.530	0.041900
13	RADIOTHERAPY AND ONCOLOGY	15,639	4.328	0.028040
14	MEDICAL IMAGE ANALYSIS	5,539	4.188	0.010720
15	EUROPEAN RADIOLOGY	16,381	3.967	0.033340
16	IEEE TRANSACTIONS ON MEDICAL IMAGING	15,215	3.942	0.019660
17	JOURNAL OF NUCLEAR CARDIOLOGY	3,021	3.930	0.003920
18	MAGNETIC RESONANCE IN MEDICINE	29,816	3.924	0.035960
19	CLINICAL NUCLEAR MEDICINE	4,008	3.640	0.006470
20	SEMINARS IN NUCLEAR MEDICINE	2,056	3.630	0.002800
21	AMERICAN JOURNAL OF NEURORADIOLOGY	21,720	3.550	0.032180
22	MOLECULAR IMAGING AND BIOLOGY	2,228	3.466	0.005880
23	ULTRASCHALL IN DER MEDIZIN	1,907	3.452	0.003930
24	RADIOGRAPHICS	10,286	3.427	0.009660
25	Biomedical Optics Express	6,187	3.337	0.021610
26	Contrast Media & Molecular Imaging	1,131	3.307	0.002810
27	INTERNATIONAL JOURNAL OF HYPERTHERMIA	3,030	3.262	0.003810

Publication C: Quantifying the Effect of Slice Thickness, Intravenous Contrast and Tube Current on Muscle Segmentation: Implications for Body Composition Analysis

Fuchs G, Chretien YR, Mario J, Do S, Eikermann M, Liu B, Yang K, Fintelmann FJ. *European Radiology*. 2018;28(6):2455-2463.

https://doi.org/10.1007/s00330-017-5191-3

Journal Data Filtered By: **Selected JCR Year: 2018** Selected Editions: SCIE,SSCI Selected Categories: **"RADIOLOGY, NUCLEAR MEDICINE and MEDICAL IMAGING"** Selected Category Scheme: WoS

Gesamtanzahl: 129 Journale

Rank	Full Journal Title	Total Cites	Journal Impact Factor	Eigenfactor Score
1	JACC-Cardiovascular Imaging	8,801	10.975	0.026160
2	MEDICAL IMAGE ANALYSIS	7,694	8.880	0.013370
3	IEEE TRANSACTIONS ON MEDICAL IMAGING	19,545	7.816	0.024990
4	RADIOLOGY	54,641	7.608	0.061300
5	JOURNAL OF NUCLEAR MEDICINE	27,551	7.354	0.037990
6	EUROPEAN JOURNAL OF NUCLEAR MEDICINE AND MOLECULAR IMAGING	15,406	7.182	0.024760
7	CLINICAL NUCLEAR MEDICINE	4,922	6.498	0.007680
8	INTERNATIONAL JOURNAL OF RADIATION ONCOLOGY BIOLOGY PHYSICS	45,833	6.203	0.046810
9	INVESTIGATIVE RADIOLOGY	6,563	6.091	0.011150
10	Circulation-Cardiovascular Imaging	5,456	5.813	0.018480
11	NEUROIMAGE	99,720	5.812	0.132720
12	ULTRASOUND IN OBSTETRICS & GYNECOLOGY	12,336	5.595	0.020140
13	European Heart Journal-Cardiovascular Imaging	5,498	5.260	0.021650
14	RADIOTHERAPY AND ONCOLOGY	17,873	5.252	0.027470
15	Photoacoustics	512	5.250	0.001330
16	JOURNAL OF CARDIOVASCULAR MAGNETIC RESONANCE	5,113	5.070	0.014020
17	ULTRASCHALL IN DER MEDIZIN	2,238	4.613	0.003700
18	HUMAN BRAIN MAPPING	22,040	4.554	0.043230
19	JOURNAL OF NUCLEAR CARDIOLOGY	3,711	4.112	0.004480
20	EUROPEAN RADIOLOGY	19,597	3.962	0.033870

Rank	Full Journal Title	Total Cites	Journal Impact Factor	Eigenfactor Score
21	RADIOGRAPHICS	11,768	3.923	0.009170
22	Biomedical Optics Express	9,547	3.910	0.021750
23	MAGNETIC RESONANCE IN MEDICINE	32,648	3.858	0.034990
24	SEMINARS IN NUCLEAR MEDICINE	2,245	3.798	0.002710
25	Journal of the American College of Radiology	4,191	3.785	0.009760
26	JOURNAL OF MAGNETIC RESONANCE IMAGING	17,147	3.732	0.027800
27	KOREAN JOURNAL OF RADIOLOGY	2,687	3.730	0.004800
28	INTERNATIONAL JOURNAL OF HYPERTHERMIA	3,552	3.589	0.004020
29	EJNMMI Physics	394	3.475	0.001350
30	NMR IN BIOMEDICINE	7,511	3.414	0.014790
31	MOLECULAR IMAGING AND BIOLOGY	2,543	3.341	0.005360
32	Journal of Cardiovascular Computed Tomography	1,711	3.316	0.004430
33	COMPUTERIZED MEDICAL IMAGING AND GRAPHICS	2,464	3.298	0.002990
34	AMERICAN JOURNAL OF NEURORADIOLOGY	23,231	3.256	0.028010
35	MEDICAL PHYSICS	26,715	3.177	0.030870
36	AMERICAN JOURNAL OF ROENTGENOLOGY	33,633	3.161	0.028540
37	CANCER IMAGING	1,406	3.153	0.002220
38	Quantitative Imaging in Medicine and Surgery	1,072	3.074	0.002420
39	PHYSICS IN MEDICINE AND BIOLOGY	27,458	3.030	0.031970
40	EJNMMI Research	1,408	3.000	0.004320
41	EUROPEAN JOURNAL OF RADIOLOGY	12,871	2.948	0.019480
42	Radiation Oncology	5,669	2.895	0.012980

Publication D: Significance of Acquisition Parameters for Adipose Tissue Segmentation on CT Images

Troschel AS, Troschel FM, Fuchs G, Marquardt JP, Ackman JB, Yang K, Fintelmann FJ. *American Journal of Roentgenology*. 2021;217(1):177-185.

https://doi.org/10.2214/AJR.20.23280

Journal Data Filtered By: **Selected JCR Year: 2016** Selected Editions: SCIE,SSCI Selected Categories: **"RADIOLOGY, NUCLEAR MEDICINE and MEDICAL IMAGING"** Selected Category Scheme: WoS

Gesamtanzahl: 126 Journale

Rank	Full Journal Title	Total Cites	Journal Impact Factor	Eigenfactor Score
1	JACC-Cardiovascular Imaging	6,895	10.189	0.027050
2	RADIOLOGY	50,983	7.296	0.066140
3	EUROPEAN JOURNAL OF NUCLEAR MEDICINE AND MOLECULAR IMAGING	14,019	7.277	0.024910
4	Circulation-Cardiovascular Imaging	4,472	6.803	0.019120
5	JOURNAL OF NUCLEAR MEDICINE	24,977	6.646	0.037540
6	NEUROIMAGE	85,630	5.835	0.173210
7	JOURNAL OF CARDIOVASCULAR MAGNETIC RESONANCE	4,349	5.601	0.014950
8	SEMINARS IN RADIATION ONCOLOGY	2,232	5.356	0.003910
9	INVESTIGATIVE RADIOLOGY	5,925	5.195	0.011230
10	INTERNATIONAL JOURNAL OF RADIATION ONCOLOGY BIOLOGY PHYSICS	44,068	5.133	0.060060
11	ULTRASOUND IN OBSTETRICS & GYNECOLOGY	11,611	4.710	0.019350
12	HUMAN BRAIN MAPPING	18,139	4.530	0.041900
13	RADIOTHERAPY AND ONCOLOGY	15,639	4.328	0.028040
14	MEDICAL IMAGE ANALYSIS	5,539	4.188	0.010720
15	EUROPEAN RADIOLOGY	16,381	3.967	0.033340
16	IEEE TRANSACTIONS ON MEDICAL IMAGING	15,215	3.942	0.019660
17	JOURNAL OF NUCLEAR CARDIOLOGY	3,021	3.930	0.003920
18	MAGNETIC RESONANCE IN MEDICINE	29,816	3.924	0.035960
19	CLINICAL NUCLEAR MEDICINE	4,008	3.640	0.006470
20	SEMINARS IN NUCLEAR MEDICINE	2,056	3.630	0.002800
21	AMERICAN JOURNAL OF NEURORADIOLOGY	21,720	3.550	0.032180
22	MOLECULAR IMAGING AND BIOLOGY	2,228	3.466	0.005880
23	ULTRASCHALL IN DER MEDIZIN	1,907	3.452	0.003930
24	RADIOGRAPHICS	10,286	3.427	0.009660
25	Biomedical Optics Express	6,187	3.337	0.021610
26	Contrast Media & Molecular Imaging	1,131	3.307	0.002810
27	INTERNATIONAL JOURNAL OF HYPERTHERMIA	3,030	3.262	0.003810

Rank	Full Journal Title	Total Cites	Journal Impact Factor	Eigenfactor Score
28	Journal of Cardiovascular Computed Tomography	1,331	3.185	0.004220
29	JOURNAL OF MAGNETIC RESONANCE IMAGING	15,073	3.083	0.029170
30	Journal of the American College of Radiology	2,690	2.993	0.006840
31	NMR IN BIOMEDICINE	6,766	2.872	0.014560
32	JOURNAL OF VASCULAR AND INTERVENTIONAL RADIOLOGY	8,371	2.780	0.012840
33	AMERICAN JOURNAL OF ROENTGENOLOGY	31,676	2.778	0.035740
34	PHYSICS IN MEDICINE AND BIOLOGY	22,873	2.742	0.034390
35	STRAHLENTHERAPIE UND ONKOLOGIE	2,687	2.735	0.004990
36	Clinical Neuroradiology	433	2.618	0.001550
37	MEDICAL PHYSICS	22,942	2.617	0.037250
38	Radiation Oncology	4,358	2.568	0.013680
39	RADIATION RESEARCH	8,394	2.539	0.007920
40	JOURNAL OF BIOMEDICAL OPTICS	12,700	2.530	0.024520
41	JOURNAL OF NEURORADIOLOGY	792	2.526	0.001310
42	ULTRASOUND IN MEDICINE AND BIOLOGY	9,759	2.494	0.012640
43	QUARTERLY JOURNAL OF NUCLEAR MEDICINE AND MOLECULAR IMAGING	1,030	2.481	0.001800
44	CLINICAL RADIOLOGY	5,717	2.478	0.008540
45	EUROPEAN JOURNAL OF RADIOLOGY	11,328	2.462	0.026500
46	NUCLEAR MEDICINE AND BIOLOGY	3,918	2.426	0.006210
47	CANCER IMAGING	1,008	2.404	0.001930
48	RADIATION AND ENVIRONMENTAL BIOPHYSICS	1,468	2.398	0.002460
49	ULTRASONICS	5,752	2.327	0.008130
50	Diagnostic and Interventional Imaging	957	2.277	0.002420
51	MAGNETIC RESONANCE IMAGING	6,465	2.225	0.011370
52	CARDIOVASCULAR AND INTERVENTIONAL RADIOLOGY	4,859	2.191	0.008890
53	KOREAN JOURNAL OF RADIOLOGY	1,941	2.156	0.003730
54	ACADEMIC RADIOLOGY	4,804	2.128	0.009150
55	NEURORADIOLOGY	5,191	2.093	0.007520
56	Dose-Response	671	2.088	0.001310
57	Brachytherapy	1,442	2.082	0.003540
58	BRITISH JOURNAL OF RADIOLOGY	7,990	2.050	0.011760
59	EJNMMI Research	844	2.033	0.003380

Rank	Full Journal Title	Total Cites	Journal Impact Factor	Eigenfactor Score
60	ACTA RADIOLOGICA	4,199	2.011	0.006600
61	JOURNAL OF THORACIC IMAGING	1,265	2.010	0.002550
62	INTERNATIONAL JOURNAL OF RADIATION BIOLOGY	4,417	1.992	0.004350
63	Physica Medica-European Journal of Medical Physics	1,385	1.990	0.003530
64	INTERNATIONAL JOURNAL OF CARDIOVASCULAR IMAGING	2,742	1.896	0.007940
65	RADIOLOGIC CLINICS OF NORTH AMERICA	2,330	1.890	0.002560
66	Diagnostic and Interventional Radiology	1,029	1.886	0.002530
67	International Journal of Computer Assisted Radiology and Surgery	1,474	1.863	0.003300
68	ABDOMINAL IMAGING	3,246	1.842	0.006240
69	Radiologia Medica	1,881	1.795	0.003430
70	JOURNAL OF RADIATION RESEARCH	2,270	1.788	0.004620
71	ULTRASONIC IMAGING	1,040	1.780	0.000750
72	COMPUTERIZED MEDICAL IMAGING AND GRAPHICS	1,800	1.738	0.002530
73	SKELETAL RADIOLOGY	5,263	1.737	0.009010
74	MAGNETIC RESONANCE MATERIALS IN PHYSICS BIOLOGY AND MEDICINE	1,391	1.718	0.002840
75	CANCER BIOTHERAPY AND RADIOPHARMACEUTICALS	1,567	1.689	0.002330
76	Radiology and Oncology	604	1.681	0.001500
77	JOURNAL OF NEUROIMAGING	1,772	1.664	0.004420
78	JOURNAL OF RADIOLOGICAL PROTECTION	974	1.657	0.001970
79	DENTOMAXILLOFACIAL RADIOLOGY	2,076	1.594	0.003040
80	JOURNAL OF ULTRASOUND IN MEDICINE	6,094	1.547	0.007920
81	Zeitschrift fur Medizinische Physik	450	1.531	0.001220
82	Journal of Contemporary Brachytherapy	332	1.496	0.000630
83	Molecular Imaging	1,135	1.479	0.001900
84	NUCLEAR MEDICINE COMMUNICATIONS	2,752	1.472	0.004640
85	PEDIATRIC RADIOLOGY	5,489	1.465	0.007820
86	Magnetic Resonance Imaging Clinics of North America	870	1.446	0.001490
87	ROFO-FORTSCHRITTE AUF DEM GEBIET DER RONTGENSTRAHLEN UND DER BILDGEBENDEN VERFAHREN	1,428	1.418	0.002530

Rank	Full Journal Title	Total Cites	Journal Impact Factor	Eigenfactor Score
88	JOURNAL OF DIGITAL IMAGING	1,518	1.407	0.002650
89	ANNALS OF NUCLEAR MEDICINE	1,980	1.396	0.003440
90	JOURNAL OF COMPUTER ASSISTED TOMOGRAPHY	5,549	1.394	0.005280
91	SEMINARS IN MUSCULOSKELETAL RADIOLOGY	705	1.374	0.001340
92	Journal of Applied Clinical Medical Physics	1,775	1.338	0.004390
93	NEUROIMAGING CLINICS OF NORTH AMERICA	1,017	1.325	0.001350
94	HEALTH PHYSICS	4,176	1.276	0.003730
95	CANADIAN ASSOCIATION OF RADIOLOGISTS JOURNAL-JOURNAL DE L ASSOCIATION CANADIENNE DES RADIOLOGISTES	489	1.266	0.000890
96	Journal of Medical Imaging and Radiation Oncology	945	1.189	0.002740
97	SEMINARS IN INTERVENTIONAL RADIOLOGY	863	1.150	0.001480
98	Magnetic Resonance in Medical Sciences	606	1.141	0.001160
99	SEMINARS IN ULTRASOUND CT AND MRI	828	1.130	0.001240
100	APPLIED RADIATION AND ISOTOPES	7,005	1.128	0.008660
101	Journal of Innovative Optical Health Sciences	355	1.120	0.000810
102	Medical Ultrasonography	492	1.118	0.001330
103	NUKLEARMEDIZIN-NUCLEAR MEDICINE	534	1.087	0.000970
104	BMC MEDICAL IMAGING	592	1.060	0.001490
105	SURGICAL AND RADIOLOGIC ANATOMY	2,583	1.051	0.003240
106	Hellenic Journal of Nuclear Medicine	347	1.048	0.000570
107	CLINICAL IMAGING	1,684	1.015	0.003420
108	Japanese Journal of Radiology	797	0.982	0.002260
109	Medical Dosimetry	687	0.957	0.001110
110	Revista Espanola de Medicina Nuclear e Imagen Molecular	386	0.951	0.000720
111	Cancer Radiotherapie	780	0.930	0.001060
112	RADIATION PROTECTION DOSIMETRY	5,723	0.917	0.007160
113	JOURNAL OF CLINICAL ULTRASOUND	2,012	0.906	0.001950
114	Ultrasound Quarterly	461	0.902	0.000790
115	INTERVENTIONAL NEURORADIOLOGY	900	0.739	0.001590
116	SEMINARS IN ROENTGENOLOGY	423	0.667	0.000500

J Digit Imaging (2017) 30:487–498
DOI 10.1007/s10278-017-9988-z

Pixel-Level Deep Segmentation: Artificial Intelligence Quantifies Muscle on Computed Tomography for Body Morphometric Analysis

Hyunkwang Lee[1] · Fabian M. Troschel[1] · Shahein Tajmir[1] · Georg Fuchs[2] · Julia Mario[1] · Florian J. Fintelmann[1] · Synho Do[1]

Published online: 26 June 2017

Abstract Pretreatment risk stratification is key for personalized medicine. While many physicians rely on an "eyeball test" to assess whether patients will tolerate major surgery or chemotherapy, "eyeballing" is inherently subjective and difficult to quantify. The concept of morphometric age derived from cross-sectional imaging has been found to correlate well with outcomes such as length of stay, morbidity, and mortality. However, the determination of the morphometric age is time intensive and requires highly trained experts. In this study, we propose a fully automated deep learning system for the segmentation of skeletal muscle cross-sectional area (CSA) on an axial computed tomography image taken at the third lumbar vertebra. We utilized a fully automated deep segmentation model derived from an extended implementation of a fully convolutional network with weight initialization of an ImageNet pre-trained model, followed by post processing to eliminate intramuscular fat for a more accurate analysis. This experiment was conducted by varying window level (WL), window width (WW), and bit resolutions in order to better understand the effects of the parameters on the model performance. Our best model, fine-tuned on 250 training images and ground truth labels, achieves 0.93 ± 0.02 Dice similarity coefficient (DSC) and 3.68 ± 2.29% difference between predicted and ground truth muscle CSA on 150 held-out test cases. Ultimately, the fully automated segmentation system can be embedded into the clinical environment to accelerate the quantification of muscle and expanded to volume analysis of 3D datasets.

Keywords Muscle segmentation · Convolutional neural networks · Computer-aided diagnosis (CAD) · Computed tomography · Artificial intelligence · Deep learning

Introduction

Image segmentation, also known as pixel-level classification, is the process of partitioning all pixels in an image into a finite number of semantically non-overlapping segments. In medical imaging, image segmentation has been considered a fundamental process for various medical applications including disease

✉ Synho Do
sdo@mgh.harvard.edu

Hyunkwang Lee
hlee51@mgh.harvard.edu

Fabian M. Troschel
ftroschel@mgh.harvard.edu

Shahein Tajmir
stajmir@mgh.harvard.edu

Georg Fuchs
Georg.Fuchs@Charite.de

Julia Mario
Julia_Mario@hms.harvard.edu

Florian J. Fintelmann
fintelmann@mgh.harvard.edu

[1] Department of Radiology, Massachusetts General Hospital, 25 New Chardon Street, Suite 400B, Boston, MA 02114, USA

[2] Department of Radiology, Charite - Universitaetsmedizin Berlin, Chariteplatz 1, 10117 Berlin, Germany

diagnosis, prognosis, and treatments. In particular, muscle segmentation on computed tomography (CT) for body composition analysis has emerged as a clinically useful risk stratification tool in oncology [1–3], radiation oncology [4], intensive care [5, 6], and surgery [7–10]. Cadaver studies have established muscle cross-sectional area (CSA) at the level of the third lumbar (L3) vertebral body as a surrogate marker for lean body muscle mass [11, 12]. These studies applied semi-automated threshold-based segmentation with pre-defined Hounsfield unit (HU) ranges to separate lean muscle mass from fat. However, segmentation errors require manual correction based on visual analysis by highly skilled radiologists [13]. As a result, semi-automated body composition analysis on large datasets is impractical due to the expense and time required. Thus, there is a role for automated tissue segmentation in order to bring body composition analysis into clinical practice.

Adipose tissue segmentation on CT images is a relatively straightforward process as fat can be thresholded with a consistent HU range [−190 to −30] [14]. Muscle segmentation is less straightforward as muscle and neighboring organs have overlapping HU values [−29 to 150]. Few published strategies exist for automated muscle segmentation with various approaches. A series of publications by Kamiya et al. [15–17] focused on segmentation of a single muscle (psoas major) at L3. Popuri et al. have studied the segmentation of all skeletal muscles visible at the L3 [18] and T4 levels [19, 20]. Their approach involves a deformable shape model based on the ideal muscle appearance with fitting based on a statistical deformation model (SDM). Another study [21] attempted to segment a 3D body CT dataset with seven segmentation classes including fat and muscle by classifying each class using random forest classifiers when given 16 image features extracted from statistical information and filter responses. All these attempts require sophisticated hand-crafted features to define knowledge-based parameters and select constraints for well-formed statistical shape and appearance models. As a result, these approaches cannot be generalized.

Deep learning has demonstrated enormous success in improving diagnostic accuracy, speed of image interpretation, and clinical efficiency for a wide range of medical tasks, ranging from the interstitial pattern detection on chest CT [22] to bone age classification on hand radiographs [23]. Particularly, a data-driven approach with deep neural networks has been actively utilized for several medical image segmentation applications, ranging from segmenting brain tumors on magnetic resonance images [24–26], organs of interest on CT [27, 28], to segmenting the vascular network of the human eye on fundus photography [29]. This success is attributed to its capability to learn representative and hierarchical image features from data [30], rather than relying on manually engineered features based on knowledge from domain experts.

In this study, we propose a fully automated deep segmentation system for the segmentation of muscles on an axial CT slice taken at L3 using the improved fully convolutional network (FCN) [31] and post processing. This system enables real-time segmentation of muscle and possibly fat tissue, facilitating clinical application of body morphological analysis sets.

Method

Dataset

Data Acquisition and Characteristics

IRB approval was obtained for this retrospective study. Four hundred patients with an abdominal CT and lung cancer treated with either surgery or systemic therapy between 2007 and 2015 were identified in an institutional database. The surgical cohort (tumor stages I, II, and III) represented a cross section of all patients who underwent lung cancer resection at our institution, while the medical cohort were patients who received chemotherapy (tumor stage IV). Only examinations with intravenous contrast were included to ensure consistency of HU values. Four hundred examinations of 200 females and 200 male patients were included in the study, as detailed in Table 1. A test subset of 150 cases was created for evaluating the algorithm performance by taking 25 cases from each BMI category per gender, as explained in "Data Categorization."

Images were acquired for routine clinical care as detailed in Table 2. Scanners were calibrated daily using manufacturer-supplied phantoms to ensure consistency in attenuation

Table 1 Patient characteristics of the entire cohort ($n = 400$) and the test subset ($n = 150$)

Patient characteristics	$n = 400$ (entire cohort)	$n = 150$ (test subset)	p values
Age, mean (SD) (years)	63 (12)	62 (11)	0.31
Gender, no. (%)			1
Female	200 (50)	75 (50)	
Male	200 (50)	75 (50)	
Height, mean (SD) (cm)	168 (10)	168 (10)	0.70
Weight, mean (SD) (kg)	77 (18)	79 (19)	0.16
Lung cancer treatment, no. (%)			0.78
Systemic therapy	227 (57)	86 (57)	
Surgery	173 (43)	64 (43)	
Lung cancer stage, no. (%)			0.84
I	102 (26)	38 (25)	
II	33 (8)	10 (7)	
III	38 (10)	16 (11)	
IV	227 (57)	86 (57)	

Note that there is no statistically significant difference between the entire cohort and the test subset

measurements in accordance with manufacturer specifications. Full resolution 512 × 512 pixel diagnostic quality CT examinations were loaded onto a research workstation running OsiriX without downsampling (Pixmeo, Bernex, Switzerland). Segmentation maps of skeletal muscle CSA at the level of L3 were created on a single axial image using semi-automated threshold-based segmentation (thresholds −29 to +150 HU). Analyzed muscles included the transversus abdominis, external and internal abdominal obliques, rectus abdominis, erector spinae, psoas major and minor, and quadratus lumborum. A research assistant (initials [JM]) blinded to all other data created the segmentation maps. *All cases were reviewed and corrected as necessary by a fellowship-trained board-certified radiologist* (*initials* [*FJF*] *with 8-years of experience*). A subset of the images were randomly selected and then re-analyzed by a second research assistant (initials [GF]) with an inter-analyst agreement of 0.998. These muscle segmentation maps were used for ground truth labeling during training, testing, and verification.

Data Preparation

We reformatted the manually tuned muscle segmentation maps created by domain experts as described previously into acceptable input for convolutional neural networks (CNN). As shown in Fig. 1, the axial images and their corresponding color-coded images served as original input data and ground truth labels, respectively. The main challenge for muscle segmentation is the accurate differentiation of muscle tissue from neighboring organs due to their overlapping HU ranges. We manually drew a boundary between organs and muscle, setting the inside region as additional segmentation class ("Inside") in an effort to train the neural network to learn distinguishing features of muscle for a precise segmentation from adjacent organs. The color-coded label images were assigned to pre-defined label indices, including 0 (black) for "Background", 1 (red) for "Muscle", and 2 (green) for "Inside", before passing through CNNs for training as presented in Fig. 1.

Table 2 Image acquisition parameters

Imaging system	*n* = 400 (entire cohort)	*n* = 150 (test subset)
Tube current, mA (SD)	360.78 (124.10)	363.41 (126.85)
kV, (SD)	120.85 (5.68)	120.67 (5.85)
Oral contrast, no. (%)	191 (48)	70 (47)
Manufacturer, no. (%)		
Siemens	141 (35)	92 (35)
GE	241 (60)	52 (61)
Philips	17 (4)	6 (4)
Toshiba	1 (0)	0 (0)

Data Categorization

We hypothesized that differences in body habitus could represent a confounding feature if the network was to be presented unbalanced examples, particularly because prior work has demonstrated that obese patients have higher image noise [32]. To minimize this possibility, the patients were categorized into eight groups based on gender and body mass index (BMI) (Fig. 2). We randomly selected 25 male and 25 female patients from the groups with normal weight, overweight, and obese in order to create a subset of 150 cases to be withheld for testing. All underweight cases were included in the training dataset without being used for testing due to their small number. The other 250 cases were used for training. We chose the best model out of several trained models by selecting the last model after the loss became converged for a sufficiently long period of training time, approximately 500 epochs. The best CNN was evaluated using the held-out test datasets to determine how much the predicted muscle regions overlap with the ground truth. In order to make a fair comparison, we used the same seed value for the random selection from the test dataset for each experiment.

System Architecture

Our proposed fully automated deep segmentation system for muscle segmentation includes grayscale image conversion using the best combination of window settings and bit depth per pixel with post processing to correct erroneous segmentation (Fig. 3).

Segmentation AI: Fully Convolutional Network

Several state-of-the-art deep learning algorithms have been validated for natural image segmentation applications [31]. We chose to develop our muscle segmentation model based on a fully convolutional network (FCN) for three reasons: First, a set of convolutional structures enables learning highly representative and hierarchical abstractions from whole-image input without excessive use of trainable parameters thanks to the usage of shared weights. Second, fine-tuning the trainable parameters of the FCN after weights that are initialized with a pre-trained model from a large-scale dataset allows the network to find the global optimum with a fast convergence of cost function when given a small training dataset. Third, the FCN intentionally fuses different levels of layers by combining coarse semantic information and fine appearance information to maximize hierarchical features learned from earlier and later layers. As shown in Fig. 4, FCN-32s, FCN-16s, and FCN-8s fuse coarse-grained and fine-grained features and upsample them at strides 32, 16, and 8, for further precision. Prior implementations of FCN describe further fusion of earlier layers beyond pool3; however, this was not pursued in

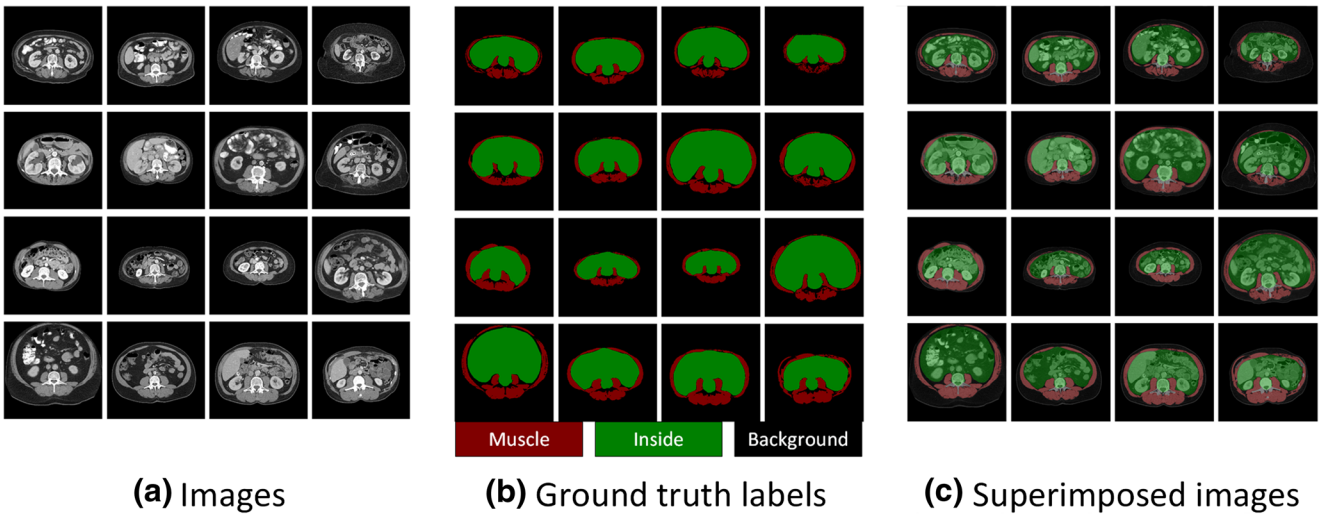

Fig. 1 Examples of (**a**) axial images and (**b**) ground truth labels used for training and testing the segmentation convolutional neural network (CNN). (**c**) Superimposed images demonstrate the target output by the CNN. Note that "*Inside*" corresponds to the entire region surrounded by muscle, including organs, fat, and vertebra

their implementation due to only minor performance gains [31]. However, we decided to extend to FCN-4s and FCN-2s (highlighted in red in Fig. 4) by fusing earlier layers further because muscle segmentation requires finer precision than stride 8.

Image Conversion: HU to Grayscale

Medical images contain 12 to 16 bits per pixel, ranging from 4096 to 65,536 shades of gray per pixel. A digital CT image has a dynamic range of 4096 gray levels per pixel (12 bits per pixel), far beyond the limits of human perception. The human observer can distinguish many hundred shades of gray, and possibly as high as 700–900, but substantially less than the 4096 gray levels in a digital CT image [33]. Displays used for diagnostic CT interpretation support at most 8 bits per pixel, corresponding to 256 gray levels per pixel. To compensate for these inherent physiologic and technical limitations, images displayed on computer monitors can be adjusted by changing the window level (WL) and window width (WW), followed by assigning values outside the window range to minimum (0) or maximum (2^{BIT}-1) value, as described in Fig. 5a. The

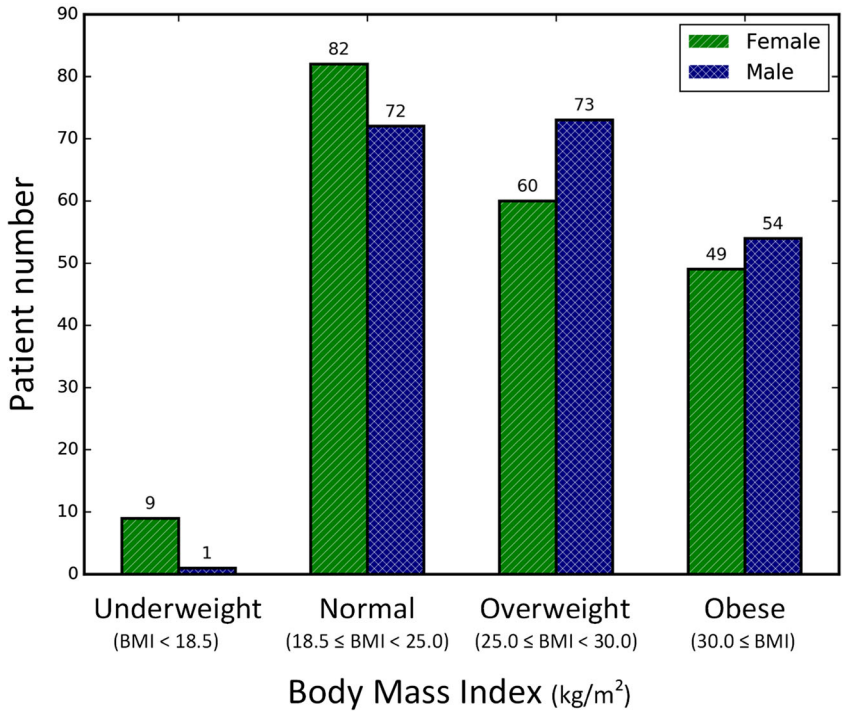

Fig. 2 Patients stratification based on gender and body mass index (BMI). For each gender, 25 cases were randomly selected from normal, overweight, and obese weight categories for the testing cohort. Underweight cases were excluded. One hundred fifty total cases were withheld for algorithm testing. The remaining cases were used to train the segmentation convolutional neural network

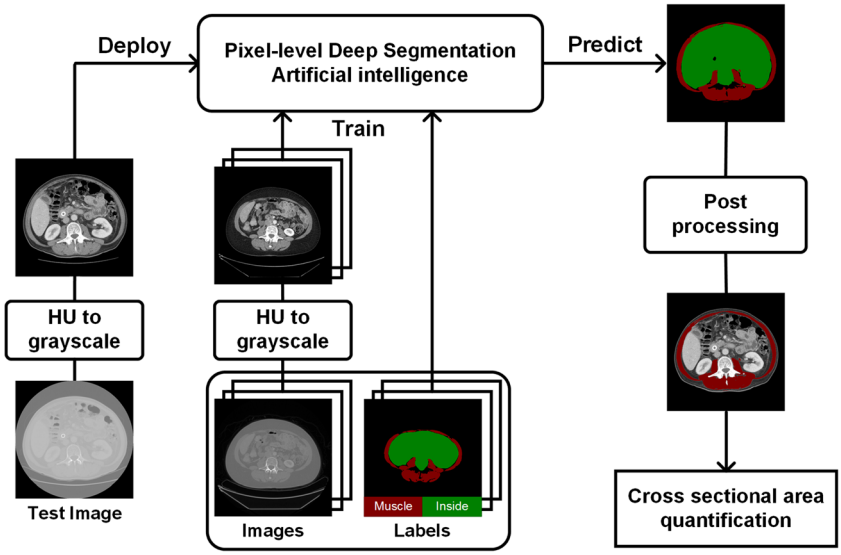

Fig. 3 Overview of proposed fully automated deep segmentation system for muscle tissue segmentation. *HU* Hounsfield units

WL—the center of the window range—determines which HU values are converted into gray levels. The WW determines how many of HU values are assigned to each gray level, related to the slope of the linear transformation shown in Fig. 5a. BIT, the available number of bits per pixel, determines how many shades of gray are available per pixel. The effects of the three configurations on image appearance are demonstrated with four examples images in Fig. 5b. The optimal window setting configuration is dependent on the HUs of the region of interest (ROI) and the intrinsic image contrast and brightness. These settings are ultimately workarounds for the constraints of human perception. However, computer vision does not necessarily have these limitations.

Most prior investigations have converted CT images to grayscale with the commonly used HU range for the target tissue or organ without studying the effect of window settings on the performance of their algorithms. While recent work has identified that image quality distortions limit the performance of neural networks [34] in computer vision systems, the effect of window setting and bit resolution on image quality is often overlooked in medical imaging machine learning. Therefore, we evaluated the effects of window and BIT settings on

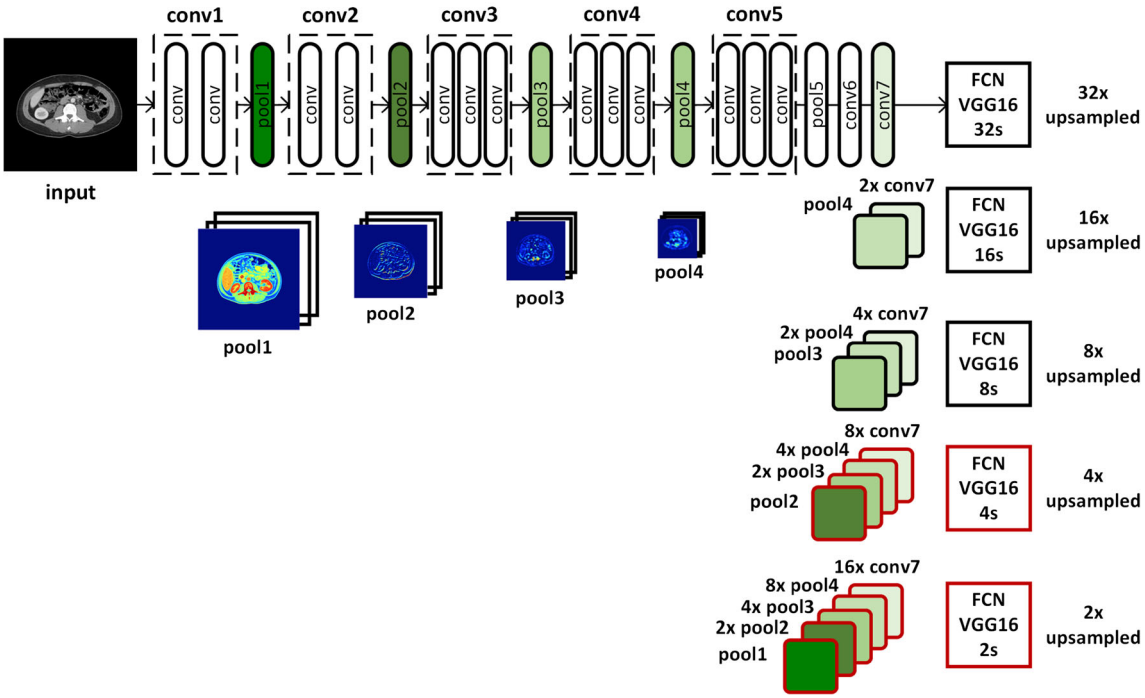

Fig. 4 Overview of the proposed fully convolutional network (FCN). FCN-32s, FCN-16s, and FCN-8s appeared in the original FCN implementation [31]. The *red-rimmed FCN-4s* and *FCN-2s* are our extended version of FCN required for more detailed and precise muscle segmentation

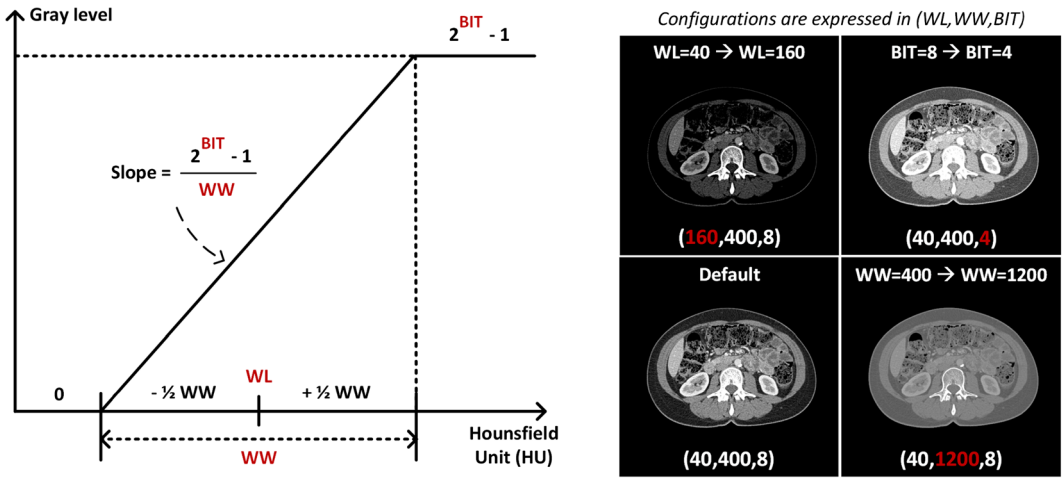

Fig. 5 (**a**) The relationship between gray level and Hounsfield units (HU) determined by window level (WL), window width (WW), and bit depth per pixel (BIT). (**b**) The effect of different WL, WW, and BIT configurations on the same image

segmentation performance by sweeping different combinations of window configurations and bit depth per pixel.

Comparison Measures

The primary comparison measure utilizes the Dice similarity coefficient (DSC) to compare the degree of overlap between the ground truth segmentation mask and the FCN-derived mask, calculated as Eq. 1.

$$\mathrm{DSC} = \frac{2 \times |ground\ truth \cap predict|}{|groiund\ truth| + |predict|} \quad (1)$$

An additional comparison measure was the cross-sectional area (CSA) error, calculated as Eq. 2. This represents a standardized measure of the percentage difference in area between the ground truth segmentation mask and the FCN-derived mask.

$$\mathrm{CSA}\ error\ (\%) = \frac{|ground\ truth - predict|}{ground\ truth} \times 100 \quad (2)$$

Intramuscular Fat Post Processing

Muscle tissue HUs do not overlap with adipose tissue HUs. As a result, a binary image of fat regions extracted using HU thresholding can be utilized to remove intramuscular fat incorrectly segmented as muscle.

Validation and Quality Control

Subsequent to post processing, the results of the test subset were visually analyzed by a research assistant together with a fellowship-trained board-certified radiologist (initials [FJF], 8 years of experience). Common errors were identified and occurrence was noted for each image.

Training

We trained the models by a stochastic gradient descent (SGD) with a momentum of 0.9 and with a minibatch size of 8 to achieve full GPU utilization. As performed in [31, 35], we utilized a fixed, tiny learning rate and weight decay because training is highly sensitive to hyperparameters when unnormalized softmax loss is used. We empirically found that a learning rate of 10^{-10} and a weight decay of 10^{-12} were optimal for our application to obtain stable training convergence at the cost of convergence speed. Since training losses eventually converged if the models were trained for sufficient period of epochs, all models in this paper were trained for 500 epochs and the last model was selected without a validation phase to evaluate performance on our held-out test subset. All experiments were run on a Devbox (NVIDIA Corp, Santa Clara, CA) containing four TITAN X GPUs with 12GB of memory per GPU [36] and using Nvidia-Caffe (version 0.15.14) and Nvidia DIGITS (version 5.1).

Statistical Analysis

Descriptive data were presented as percentages for categorical variables and as means with standard deviation (SD) for continuous variables. We used two-tailed statistical tests with the alpha level set at 0.05. We performed Student's *t* test for normally distributed values. Dichotomous variables were compared using the Mann Whitney *U* test and ordinal variables were compared using the Kruskal Wallis test. Inter-analyst agreement was quantified with intraclass correlation coefficients (ICC). All statistical analyses were performed using

STATA software (version 13.0, StataCorp, College Station, TX).

Experiments

Fully Convolutional Network

To identify the best performing fully convolutional network, five models of increasing granularity—FCN-32s, FCN-16s, FCN-8s, FCN-4s, and FCN-2s—were trained and evaluated using the test dataset at 40,400 and 8 bits per pixel by measuring the DSC and CSA error between ground truth and predicted muscle segmentation. These results were compared to the HU thresholding method, selecting HU ranging from −29 to 150 to represent lean muscle CSA.

Image Conversion: HU to Grayscale

Subsequently, we compared the performance of the best FCN model (FCN-2s) with seven different combinations of window settings for each bit depth per pixel—(40,400), (40, 240), (40,800), (40,1200), (−40,400), (100,400), and (160,400) expressed in WL and WW and 8, 6, and 4 bit resolutions per pixel. The selected window ranges cover the HU range of lean tissue [−29 to 150] for a fair comparison to see if partial image information loss degrades model performance. These window settings contain extreme window ranges as well as typical ones. For example, the window setting (40,240) has a range of −80 to 160 HU values, which corresponds to almost the HU range of lean muscle, while the configuration (40,1200) converts all HU values between −560 and 1240 into shades of gray resulting in low image contrast.

Results

FCN Segmentation Performance

The five different FCN models were compared to the previously described HU thresholding method. Performance was evaluated using the DSC and muscle CSA error and detailed in Fig. 6. Even the most coarse-grained FCN model (FCN-32s) achieved 0.79 ± 0.06 of DSC and 18.27 ± 9.77% of CSA error, markedly better than the HU thresholding method without human tuning. Performance increased as the number of features of different layers was fused. The most fine-grained FCN model achieved DSC of 0.93 and CSA error of 3.68% on average, representing a 59% improvement in DSC and an 80% decrease in CSA error when compared to the most coarse-grained model. The representative examples are detailed in Fig. 7 to visually show the performance of FCN-2s segmentation.

Effect of Window and Bit Settings on Segmentation Performance

Results of the systematic experiment comparing seven different combinations of window settings for each bit depth per pixel are presented in Fig. 8. The DSC and CSA error were not meaningfully influenced by changes in window ranges as long as 256 gray levels per pixel (bit8) were available. When 6-bit depth per pixel was used, performance was similar compared to the results of 8-bit cases. However, model performance deteriorated when 8-bit pixels were compressed to 4-bit pixels.

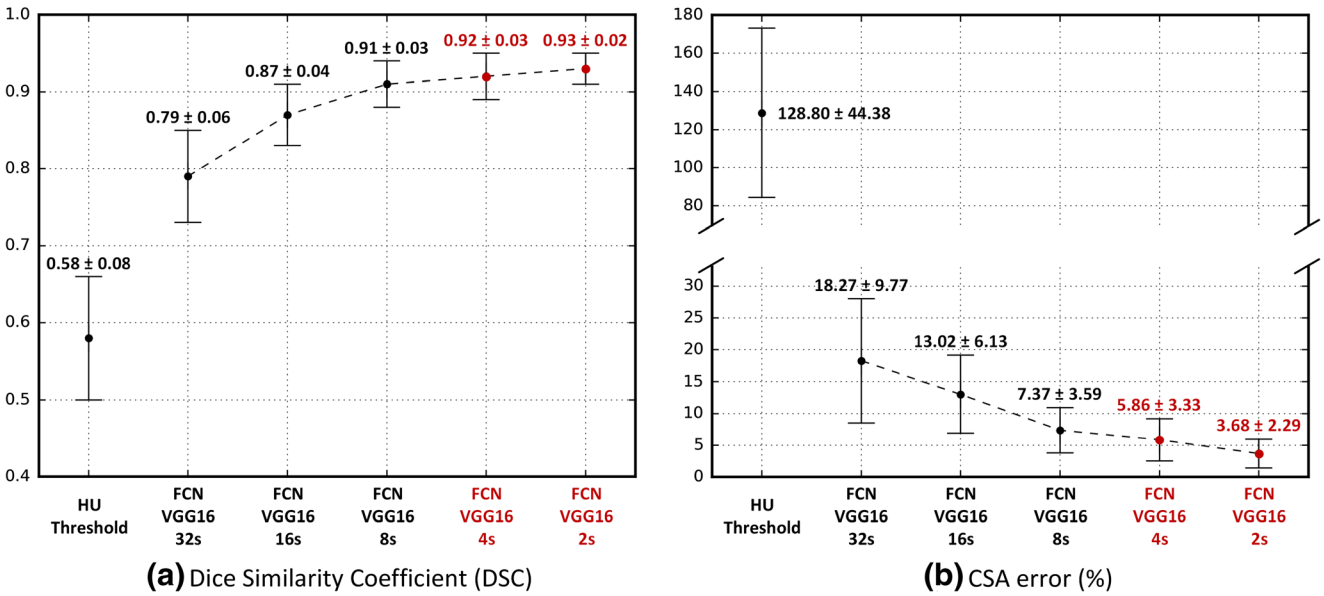

Fig. 6 Comparison of the HU thresholding method and five different FCNs. (**a**) Dice similarity coefficient (DSC) and (**b**) cross-sectional area (CSA) error between ground truth manual and predicted muscle segmentation areas. All numbers are reported as mean ± SD

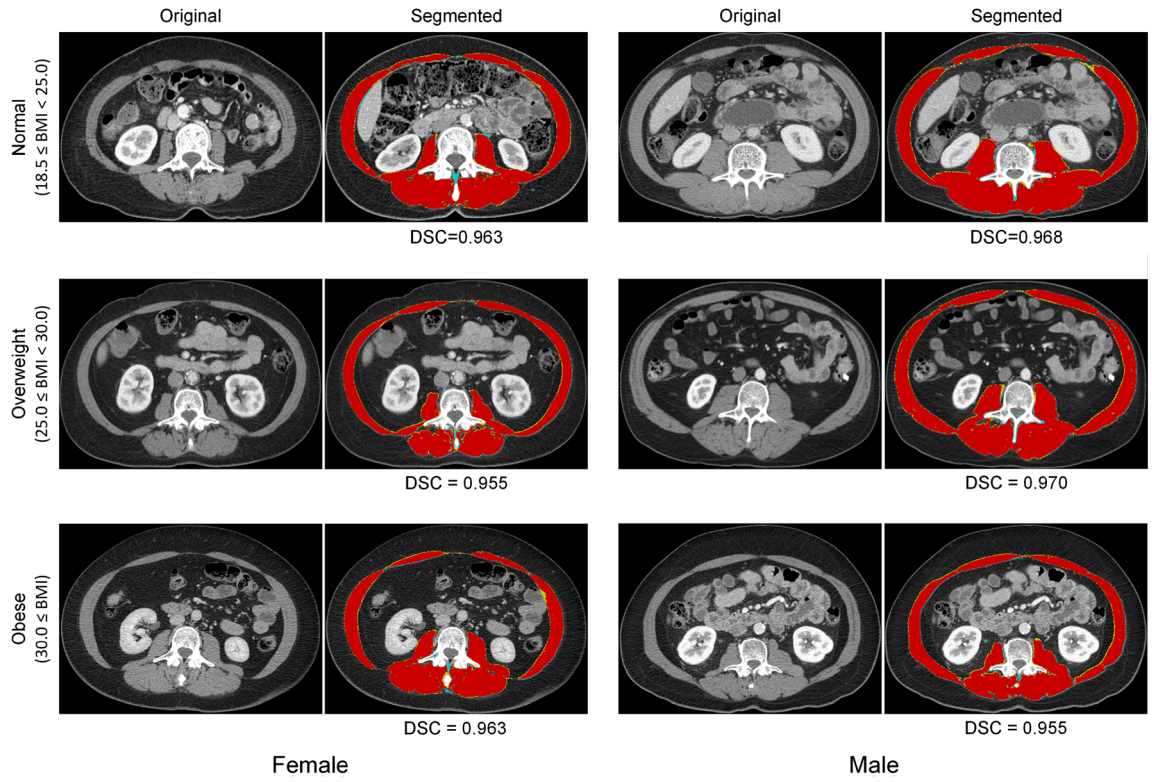

Fig. 7 Six examples of the better segmented CT images for six groups according to gender and BMI. Dice similarity coefficient (DSC) is marked on each segmented image *above*. Oversampled regions are colored in *blue*, undersampled areas are colored in *yellow*, and correctly segmented areas are colored in *red*

Deployment Time

Segmentation was performed using a single TITAN X GPU. Segmentation took 25 s on average for 150 test images, corresponding to only 0.17 s per image.

Statistical Analysis of Model Segmentation Errors

In the majority of cases ($n = 128$), FCN CSA was smaller than ground truth CSA, while only few cases resulted in oversegmentation ($n = 22$; $p < 0.0001$). Review of incorrectly

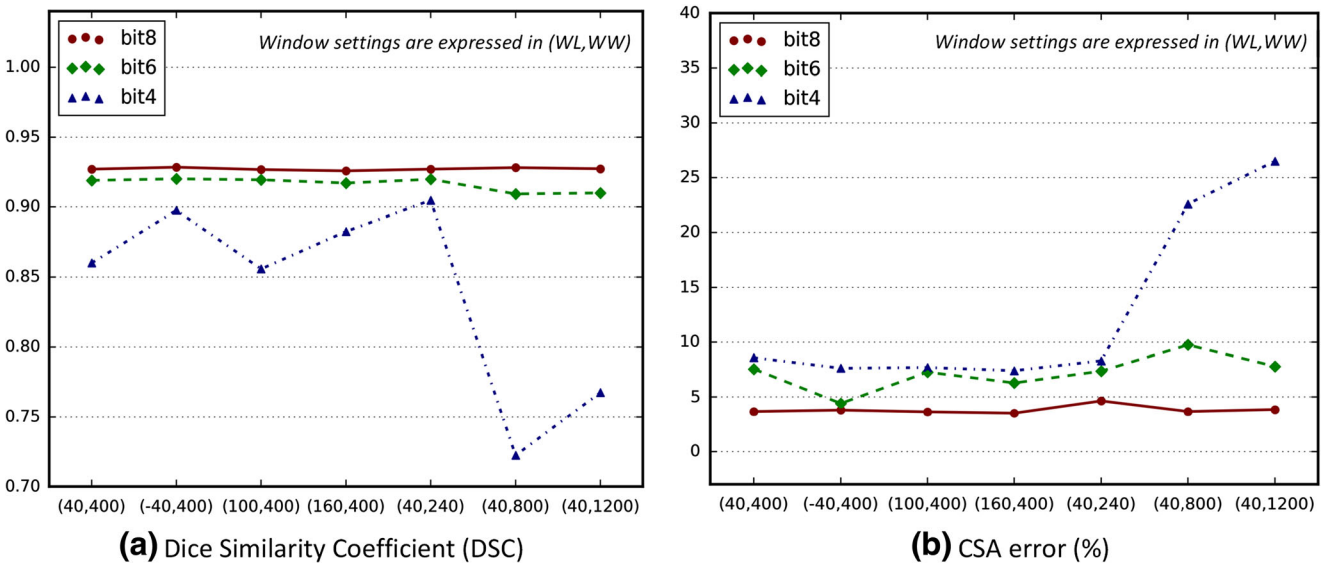

Fig. 8 Performance of FCN-2s when input images are generated with different window settings (WL, WW) for each bit depth per pixel (BIT). The selected window settings were (40,400), (−40,400), (100,400), (160,600), (40,240), (40,800), and (40,1200)

segmented images identified three main errors: incomplete muscle segmentation (n = 58; 39% of test cases), incorrect organ segmentation (n = 52; 35%), and subcutaneous edema mischaracterized as muscle (n = 17; 11% of test cases). Representative examples of these errors are demonstrated in Fig. 9.

Obesity

To evaluate the influence of obesity on the performance of the segmentation algorithm, segmentation results of patients with BMI >30 kg/m^2 were compared to those of patients with BMI <30 kg/m^2. The average DSC was 0.93 in non-obese patients, but only 0.92 in obese patients, a statistically significant difference (p = 0.0008). The incorrect inclusion of subcutaneous soft tissue edema into muscle CSA was more common in obese patients than in non-obese patients (p = 0.018). However, inclusion of adjacent organs into muscle CSA (p = 0.553) and incomplete muscle segmentation (p = 0.115) were not significantly associated with obesity. There was no statistically significant association between obesity and CSA error (p = 0.16).

Oral Contrast

Forty-eight percent of the cohort received oral contrast in addition to intravenous contrast. The ratio was the same in the training and testing datasets. There was no statistically significant association between the presence or absence of oral contrast and segmentation performance measured as DSC (p = 0.192) or CSA error (p = 0.484), probably because the network became invariant to its presence in the balanced cohorts.

Discussion

We have developed an automated system for performing muscle segmentation at the L3 vertebral body level using a fully convolutional network with post processing at a markedly faster deployment time when compared to conventional semi-automated methods.

Our model was derived from a highly granular fully convolutional network and compared to the semi-automated HU thresholding method which requires tedious and time-

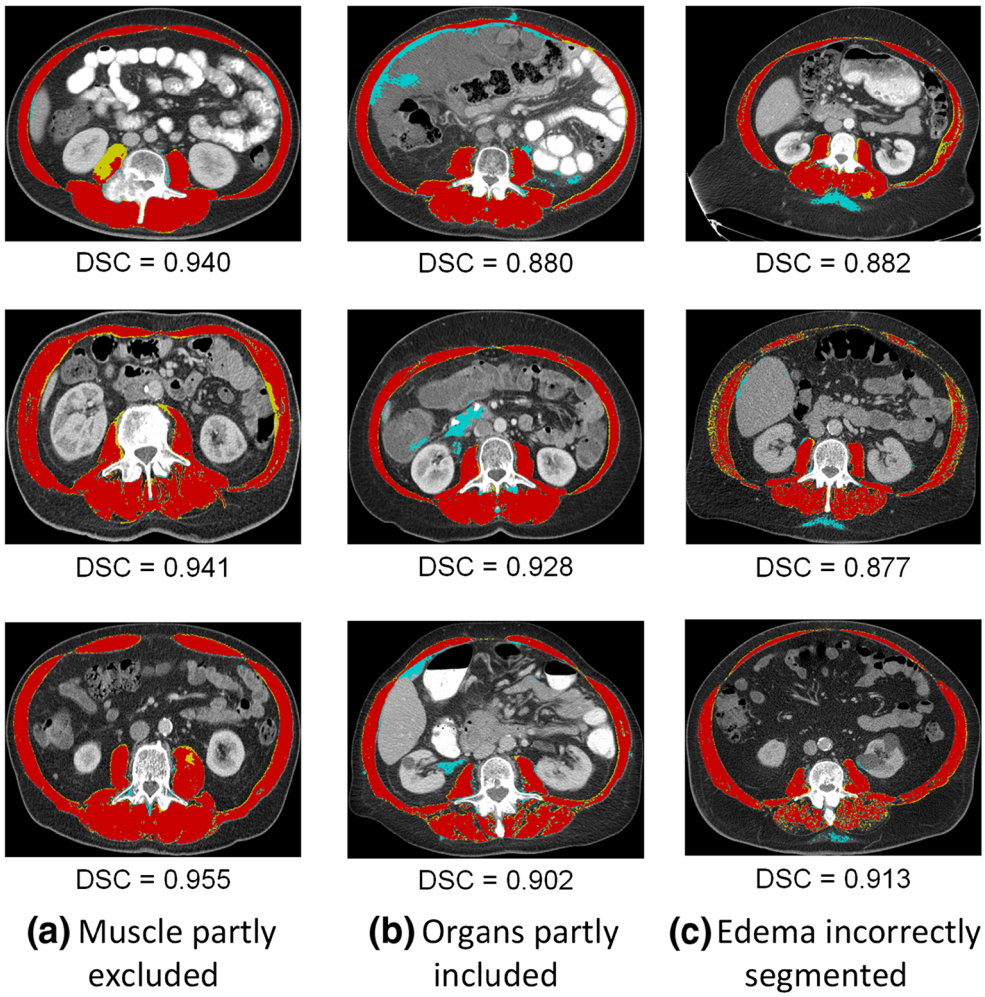

Fig. 9 Segmentation errors most commonly presented as muscle partly excluded (**a**), organs partly included (**b**), and edema mischaracterized as muscle (**c**). Oversampled regions are colored in *blue*, undersampled areas are colored in *yellow*, and correctly segmented areas are colored in *red*

consuming tuning of erroneous segmentation by highly trained human experts. When compared to the HU thresholding method without human tuning, even the coarsest FCN had markedly better performance. It is not surprising as HU thresholding is so inaccurate, as it includes overlapping HU ranges between organs and muscle. However, by combining hierarchical features and different layers of increasing granularity, our model was able to extract semantic information, overall muscle shape, fine-grained appearance, and muscle textural appearance. These results persisted even when varying the WL and WW into ranges unsuitable for the human eye. Changes in WW had greater effects on segmentation performance than WL, particularly when the number of gray shades was small (bit6 and bit4). These results imply that this network's performance depends mostly on image contrast and possibly due to the number of HU values assigned to a single gray level, rather than inherent image brightness. It also implies that preserving image information using the original 12-bit resolution with 4096 shades of gray could provide considerable performance gains by allowing the network to learn other significant identifying features of muscle which are lost in the conversion to 8 bits. These results are consistent with other published findings that CNNs are excellent at textural analysis [37, 38].

Deployment Time

Accurate segmentation of muscle tissue by the semi-automated HU thresholding method requires roughly 20–30 min per slice on average [18]. Algorithms proposed in most prior works [16, 18, 19] required between 1 and 3 min per slice. More recent works have reported that their algorithms require only 3.4 s [21] and 0.6 s per image on average. To the best of our knowledge, our model is the fastest reported segmentation algorithm for muscle segmentation and needs only 0.17 s per slice on average. Segmenting 150 test images can be performed in 25 s. This ultra-fast deployment can allow real-time segmentation in clinical practice.

Clinical Applications

Muscle CSA at L3 has been shown to correlate with a wide range of posttreatment outcomes. However, integration of muscle CSA measurements in clinical practice has been limited by the time required to generate this data. By dropping the calculation time from 1800 to 0.17 s, we can drastically speed up research into new applications for morphometric analysis. CT is an essential tool in the modern healthcare arena with approximately 82 million CT examinations performed in the USA in 2016 [39]. In lung cancer in particular, the current clinical paradigm has been on lesion detection and disease staging with an eye toward treatment selection. However, accumulating evidence suggests that CT body composition data could provide objective biological markers to help lay the foundation for the future of personalized medicine. Aside from preoperative risk stratification for surgeons, recent work has used morphometric data to predict death in radiation oncology and medical oncology [4]. Our system has the great advantage of not requiring a special protocol (other than intravenous contrast) and could derive muscle CSA from routine CT examinations near-instantaneously. This would enable body composition analysis of the vast majority of CT examinations.

Limitations

While the system has great potential for accelerating calculation of muscle CSA, there are important limitations. The network statistically tends to underestimate muscle CSA. This is probably due to a combination of overlapping HUs between muscle and adjacent organs and variable organ textural appearance. On the other end of the spectrum, segmentation is also confused by the radiographic appearance of edema particularly in obese patients, which has a similar HU range to muscle, leading to higher CSA than expected. Extensive edema tends to occur in critically ill patients, leading to potentially falsely elevated CSA in patients actually at higher risk for all interventions.

The average age of our cohort is 63 years. While this is representative of the lung cancer population, it may limit the generalizability of our system for patients with different diseases and age groups. Further training with data from a wider group of patients could enable the algorithms to account for these differences. In addition, the network should be trained to segment CT examinations performed without intravenous contrast and ultra-low radiation dose.

Future Directions

The muscle segmentation AI can be enhanced further by using the original 12-bit image resolution with 4096 gray levels which could enable the network to learn other significant determinants which could be missed in the lower resolution. In addition, an exciting target would be adipose tissue segmentation. Adipose tissue segmentation is relatively straightforward since fat can be thresholded within a unique HU range [−190 to −30]. Prior studies proposed creating an outer muscle boundary to segment HU thresholded adipose tissue into visceral adipose tissue (VAT) and subcutaneous adipose tissue (SAT). However, precise boundary generation is dependent on accurate muscle segmentation. By combining our muscle segmentation network with a subsequent adipose tissue thresholding system, we could quickly and accurately provide VAT and SAT values in addition to muscle CSA. Visceral adipose tissue has been implicated in cardiovascular outcomes and metabolic syndrome, and accurate fat segmentation would

increase the utility of our system beyond cancer prognostication [40]. Ultimately, our system should be extended to whole-body volumetric analysis rather than axial CSA, providing rapid and accurate characterization of body morphometric parameters.

Conclusion

We have created an automated, deep learning system to automatically detect and segment the muscle CSA of CT slices at the L3 vertebral body level. This system achieves excellent overlap with hand-segmented images with an average of less than 3.68% error while rapidly accelerating segmentation time from 30 min to 0.17 s. The fully automated segmentation system can be embedded into the clinical environment to accelerate the quantification of muscle to provide advanced morphometric data on existing CT volumes and possible expanded to volume analysis of 3D datasets.

References

1. Prado CMM, Lieffers JR, McCargar LJ, Reiman T, Sawyer MB, Martin L et al.: Prevalence and clinical implications of sarcopenic obesity in patients with solid tumours of the respiratory and gastrointestinal tracts: a population-based study. Lancet Oncol 9:629–635, 2008
2. Martin L, Birdsell L, Macdonald N, Reiman T, Clandinin MT, McCargar LJ et al.: Cancer cachexia in the age of obesity: skeletal muscle depletion is a powerful prognostic factor, independent of body mass index. J Clin Oncol 31:1539–1547, 2013
3. Blauwhoff-Buskermolen S, Versteeg KS, de van der Schueren MAE, den Braver NR, Berkhof J, Langius JAE et al.: Loss of muscle mass during chemotherapy is predictive for poor survival of patients with metastatic colorectal cancer. J Clin Oncol 34:1339–1344, 2016
4. McDonald AM, Swain TA, Mayhew DL, Cardan RA, Baker CB, Harris DM et al.: CT measures of bone mineral density and muscle mass can be used to predict noncancer death in men with prostate cancer. Radiology 282:475–483, 2017
5. Moisey LL, Mourtzakis M, Cotton BA, Premji T, Heyland DK, Wade CE et al.: Skeletal muscle predicts ventilator-free days, ICU-free days, and mortality in elderly ICU patients. Crit Care 17:R206, 2013
6. Weijs PJM, Looijaard WGPM, Dekker IM, Stapel SN, Girbes AR, Oudemans-van Straaten HM et al.: Low skeletal muscle area is a risk factor for mortality in mechanically ventilated critically ill patients. Crit Care 18:R12, 2014
7. Englesbe MJ, Patel SP, He K, Lynch RJ, Schaubel DE, Harbaugh C et al.: Sarcopenia and mortality after liver transplantation. J Am Coll Surg 211:271–278, 2010
8. Reisinger KW, van Vugt JLA, Tegels JJW, Snijders C, Hulsewé KWE, Hoofwijk AGM et al.: Functional compromise reflected by sarcopenia, frailty, and nutritional depletion predicts adverse postoperative outcome after colorectal cancer surgery. Ann Surg 261:345–352, 2015
9. Kuroki LM, Mangano M, Allsworth JE, Menias CO, Massad LS, Powell MA et al.: Pre-operative assessment of muscle mass to predict surgical complications and prognosis in patients with endometrial cancer. Ann Surg Oncol 22:972–979, 2015
10. Pecorelli N, Carrara G, De Cobelli F, Cristel G, Damascelli A, Balzano G et al.: Effect of sarcopenia and visceral obesity on mortality and pancreatic fistula following pancreatic cancer surgery. Br J Surg 103:434–442, 2016
11. Mitsiopoulos N, Baumgartner RN, Heymsfield SB, Lyons W, Gallagher D, Ross R: Cadaver validation of skeletal muscle measurement by magnetic resonance imaging and computerized tomography. J Appl Physiol 85:115–122, 1998
12. Shen W, Punyanitya M, Wang Z, Gallagher D, St-Onge M-P, Albu J et al.: Total body skeletal muscle and adipose tissue volumes: estimation from a single abdominal cross-sectional image. J Appl Physiol 97:2333–2338, 2004
13. Boutin RD, Yao L, Canter RJ, Lenchik L: Sarcopenia: current concepts and imaging implications. AJR Am J Roentgenol 205:W255–W266, 2015
14. Zhao B, Colville J, Kalaigian J, Curran S, Jiang L, Kijewski P et al.: Automated quantification of body fat distribution on volumetric computed tomography. J Comput Assist Tomogr 30:777–783, 2006
15. Kamiya N, Zhou X, Chen H, Hara T, Hoshi H, Yokoyama R et al.: Automated recognition of the psoas major muscles on X-ray CT images.In Engineering in Medicine and Biology Society, EMBC. 2009, pp. 3557–3560
16. Kamiya N, Zhou X, Chen H, Muramatsu C, Hara T, Yokoyama R et al.: Automated segmentation of psoas major muscle in X-ray CT images by use of a shape model: preliminary study. Radiol Phys Technol 5:5–14, 2012
17. Kamiya N, Zhou X, Chen H, Muramatsu C, Hara T, Yokoyama R et al.: Automated segmentation of recuts abdominis muscle using shape model in X-ray CT images. In Engineering in Medicine and Biology Society, EMBC. 2011, pp. 7993–7996
18. Chung H, Cobzas D, Birdsell L, Lieffers J, Baracos V: Automated segmentation of muscle and adipose tissue on CT images for human body composition analysis. SPIE Medical Imaging. International Society for Optics and Photonics 72610K–72610K–8, 2009. doi: 10.1117/12.812412
19. Popuri K, Cobzas D, Jägersand M, Esfandiari N, Baracos V: FEM-based automatic segmentation of muscle and fat tissues from thoracic CT images. 2013 I.E. 10th International Symposium on Biomedical Imaging. 2013, pp 149–152
20. Popuri K, Cobzas D, Esfandiari N, Baracos V, Jägersand M: Body composition assessment in axial CT images using FEM-based automatic segmentation of skeletal muscle. IEEE Trans Med Imaging 35:512–520, 2016
21. Polan DF, Brady SL, Kaufman RA: Tissue segmentation of computed tomography images using a random Forest algorithm: a feasibility study. Phys Med Biol 61:6553–6569, 2016
22. Anthimopoulos M, Christodoulidis S, Ebner L, Christe A, Mougiakakou S: Lung pattern classification for interstitial lung diseases using a deep convolutional neural network. IEEE Trans Med Imaging 35(5):1207–1216, 2016. doi: 10.1109/TMI.2016.2535865
23. Lee H, Tajmir S, Lee J, Zissen M, Yeshiwas BA, Alkasab TK et al.: Fully automated deep learning system for bone age assessment. J Digit Imaging 8:1–5, 2017. doi: 10.1007/s10278-017-9955-8

24. Pereira S, Pinto A, Alves V, Silva CA: Brain tumor segmentation using convolutional neural networks in MRI images. IEEE Trans Med Imaging 35(5):1240–1251, 2016. doi: 10.1109/TMI.2016.2538465
25. Havaei M, Davy A, Warde-Farley D, Biard A, Courville A, Bengio Y et al.: Brain tumor segmentation with deep neural networks. Med Image Anal 35:18–31, 2017
26. Moeskops P, Viergever MA, Mendrik AM, de Vries LS, Benders MJNL, Isgum I: Automatic segmentation of MR brain images with a convolutional neural network. IEEE Trans Med Imaging 35(5): 1252–61, 2016. doi: 10.1109/TMI.2016.2548501
27. Gao Y, Shao Y, Lian J, Wang AZ, Chen RC, Shen D: Accurate segmentation of CT male pelvic organs via regression-based deformable models and multi-task random forests. IEEE Trans Med Imaging 35:1532–1543, 2016
28. Roth HR, Lu L, Farag A, Shin H-C, Liu J, Turkbey EB et al.: Deeporgan: Multi-level deep convolutional networks for automated pancreas segmentation. In International Conference on Medical Image Computing and Computer-Assisted Intervention 2015 Oct 5, Springer International Publishing, 2015, pp. 556–564
29. Liskowski P, Pawel L, Krzysztof K: Segmenting retinal blood vessels with deep neural networks. IEEE Trans Med Imaging 35(11):2369-2380, 2016. doi:10.1109/TMI.2016.2546227
30. Greenspan H, van Ginneken B, Summers RM: Guest editorial deep learning in medical imaging: overview and future promise of an exciting new technique. IEEE Trans Med Imaging 35:1153–1159
31. Long J, Shelhamer E, Darrell T: Fully convolutional networks for semantic segmentation. Proceedings of the IEEE Conference on Computer Vision and Pattern Recognition. 3431–3440, 2015
32. Segev OL, Gaspar T, Halon DA, Peled N, Domachevsky L, Lewis BS et al.: Image quality in obese patients undergoing 256-row computed tomography coronary angiography. Int J Card Imaging 28: 633–639, 2012
33. Kimpe T, Tuytschaever T. Increasing the number of gray shades in medical display systems—how much is enough? J Digit Imaging 20:422–432, 2007
34. Dodge S, Karam L: Understanding how image quality affects deep neural networks. Quality of Multimedia Experience (QoMEX), 2016 Eighth International Conference on. IEEE 1–6. doi:10.1109/QoMEX.2016.7498955
35. Shelhamer E, Long J, Darrell T: Fully convolutional networks for semantic segmentation. IEEE Trans Pattern Anal Mach Intell 39: 640–651, 2017
36. NVIDIA® DIGITS™ DevBox. In: NVIDIA Developer [Internet]. Available: https://developer.nvidia.com/devbox, 16 Mar 2015 [cited 23 Aug 2016]
37. Cimpoi M, Maji S, Vedaldi A: Deep filter banks for texture recognition and segmentation. Proceedings of the IEEE Conference on Computer Vision and Pattern Recognition. 2015, pp 3828–3836
38. Andrearczyk V, Whelan PF: Using filter banks in convolutional neural networks for texture classification. Pattern Recogn Lett 84: 63–69, 2016
39. 2016 CT Market Outlook Report. In: IMVInfo.com [Internet]. Available: http://www.imvinfo.com/index.aspx?sec=ct&sub=dis&itemid=200081, [cited 14 Mar 2017]
40. Shuster A, Patlas M, Pinthus JH, Mourtzakis M: The clinical importance of visceral adiposity: a critical review of methods for visceral adipose tissue analysis. Br J Radiol 85:1–10, 2012

Curriculum vitae

Mein Lebenslauf wird aus datenschutzrechtlichen Gründen in der elektronischen Version meiner Arbeit nicht veröffentlicht.

Complete list of publications

First authorship:

A Fuchs G, Thevathasan T, Chretien YR, Mario J, Piriyapatsom A, Schmidt U, Eikermann M, Fintelmann FJ. **Lumbar Skeletal Muscle Index Derived from Routine Computed Tomography Exams Predict Adverse Post-Extubation Outcomes in Critically Ill Patients.** *Journal of Critical Care.* 2018;44:117-123.
Impact factor: 2.65

B Nipp RD, Fuchs G, El-Jawahri A, Mario J, Troschel FM, Greer JA, Gallagher ER, Jackson VA, Kambadakone A, Hong TS, Temel JS, Fintelmann FJ. **Sarcopenia Is Associated with Quality of Life and Depression in Patients with Advanced Cancer.** *Oncologist.* 2018;23(1):97-104.
Impact factor: 4.96

C Fuchs G, Chretien YR, Mario J, Do S, Eikermann M, Liu B, Yang K, Fintelmann FJ. **Quantifying the Effect of Slice Thickness, Intravenous Contrast and Tube Current on Muscle Segmentation: Implications for Body Composition Analysis.** *European Radiology.* 2018;28(6):2455-2463.
Impact factor: 3.97

Co-authorship:

D Troschel AS, Troschel FM, Fuchs G, Marquardt JP, Ackman JB, Yang K, Fintelmann FJ. **Significance of Acquisition Parameters for Adipose Tissue Segmentation on CT Images.** *American Journal of Roentgenology.* 2021;217(1):177-185.
Impact factor: 3.16

E Lee H, Troschel FM, Tajmir S, Fuchs G, Mario J, Fintelmann FJ, Do S. **Pixel-Level Deep Segmentation: Artificial Intelligence Quantifies Muscle on Computed Tomography for Body Morphometric Analysis.** *Journal of Digital Imaging.* 2017;30(4):487-498.
Impact factor: 1.41

Acknowledgment

I would like to express my sincere gratitude to my doctoral supervisors Prof. Dr. med. Florian J. Fintelmann, Prof. Dr. med. Bernhard Gebauer, and Prof. Dr. med. Patrick Asbach for their mentoring, guidance, and support throughout my MD/PhD. Thank you very much for the opportunity to pursue my MD/PhD project abroad in the United States and for giving me the freedom to develop my own ideas and projects. This journey has taught me many valuable lessons, from study design and statistical analysis to scientific curiosity and perseverance. Your patience and scientific enthusiasm have inspired me.

All of this would not have been possible without the wholehearted encouragement from my family Anke Fuchs, Anne Fuchs, Andreas Fuchs, and Melanie König. Thank you for believing in me always. I am very grateful to my friends who supported me on this journey and continue to inspire me time and again: Dennis Hartung, Laura Geurtz, Malte Casper, Christopher Murray, Dayton McMillan, Simone Sasse, Constantin Voll, and the many other great friends that I met along the journey in Boston and Berlin.

I am lucky to be part of the Fintelmann Lab and to have worked alongside great team members that made my MD/PhD projects exciting: Yves Chretien, Julia Mario, Amelie Troschel and Fabian Troschel. Thank you for all the help, discussions, and constructive criticism.

I would also like to express my sincere gratitude to the German Academic Scholarship Foundation and the Rolf W. Günther Foundation for their generous support of my MD/PhD projects abroad.